ՀՀ ԿՐԹՈՒԹՅԱՆ, ԳԻՏՈՒԹՅԱՆ ՄՇԱԿՈՒՅԹԻ ԵՎ ՍՊՈՐՏԻ ՆԱԽԱՐԱՐՈՒԹՅՈՒՆ
ԵՐԵՎԱՆԻ ՊԵՏԱԿԱՆ ՀԱՄԱԼՍԱՐԱՆ

Սահակյան Նարեկ Վարդանի

Բլազարների բազմաալիքային և նեյտրինային ճառագայթման ուսումնասիրությունը։

Ա.04.02 - «Տեսական ֆիզիկա» մասնագիտությամբ
ֆիզիկամաթեմատիկական գիտությունների դոկտորի
գիտական աստիճանի հայցման ատենախոսության

ԱՆՁՆԱԳԻՐ

ԵՐԵՎԱՆ-2022

THE MINISTRY OF EDUCATION, SCIENCE, CULTURE AND SPORTS OF THE RA
YEREVAN STATE UNIVERSITY

Sahakyan Narek

Study of Multiwavelength and Neutrino
Emission from Blazars

Thesis for the degree of Doctor of physical and mathematical sciences
Specialty 01.04.02 -" Theoretical Physics"

Abstract

YEREVAN–2022

Ատենախոսության թեման հաստատվել է ԵՊՀ ռադիոֆիզիկայի ֆակուլտետի գիտական խորհրդում:

Պաշտոնական ընդդիմախոսներ՝ ֆիզ.-մաթ. գիտ. դոկտոր, պրոֆեսոր Ա. Ա. Սահարյան
ֆիզ.-մաթ. գիտ. դոկտոր Գ. Տ. Տեր-Ղազարյան
ֆիզ.-մաթ. գիտ. դոկտոր, պրոֆեսոր Գ. Վերեշչագին

Առաջատար կազմակերպություն՝ ՀՀ ԳԱԱ Վ. Համբարձումյանի անվան Բյուրականի աստղադիտարան

Պաշպանությունը կայանալու է 2022 թ. հունիսի 25-ին ժամը 12-ին, Երևանի Պետական Համալսարանում գործող Ֆիզիկայի 049 Մասնագիտական խորհրդի նիստում (Երևան, 0025, Ալեք Մանուկյան 1):

Ատենախոսությանը կարելի է ծանոթանալ ԵՊՀ-ի գրադարանում:

Սեղմագիրը առաքված է 2022 մայիսի 13-ին:

Մասնագիտական խորհրդի գիտական քարտուղար՝ ֆիզ.-մաթ. գիտ. թեկնածու, դոցենտ Վ.Պ. Քալանթարյան

The thesis theme is approved at the Academic Council of the Radiophysics Department of the Yerevan State University

Official opponents: Doctor of Phys. Math. Sciences, Prof. A. A. Saharian
Doctor of Phys. Math. Sciences G. T. Ter-KazarIan
Doctor of Phys. Math. Sciences, Prof. G. Vereshchagin

Leading organization: V. Ambartsumian Byurakan Astrophysical Observatory of RA NAS

The defense of the thesis will take place at 12:00 on 25 June 2022 on the session of the Specialized Council 049 Physics of the Yerevan State University.

Address: 1 Alek Manukyan Street, 0025 Yerevan, Armenia.

The thesis is available in the library of the Yerevan State University.

The abstract is distributed on 13 May 2022.

Scientific secretary of the Specialized Council Candidate of Phys. Math. Sciences, Associate Prof. V.P. Kalantaryan

GENRAL DESCRIPTION OF THE WORK

Relevance of the topic

The Universe has always been an object of interest for the human kind. A tremendous progress in understanding of the Universe has been achieved due to the advancement in the technical capabilities of the ground- and satellite-based observatories. Now the emission from different cosmic sources can be investigated by detecting photons with energies ranging from radio to γ-rays (multiwavelength astrophysics). These multiwavelength observations provide a comprehensive view of the physical processes and allow to test models in ways never possible before. The recent detection of neutrinos from a blazar opened a new era in the astrophysics – multi-messenger astrophysics, when the same source is studied by detecting different messengers. Each of these messengers carries unique information on the physical processes and their combination provides the best chance for investigation of different sources. This opens new horizons for studying of the extreme Universe, and the multiwavelength/multi-messenger astrophysics is becoming a major and fast developing field of science.

A remarkably large number of source classes discovered to date are confirmed to have a nonthermal spectrum ranging from radio to High and Very High Energy (HE; > 100 MeV, VHE; > 100 GeV) γ-ray bands. These include Galactic sources such as pulsars, supernova remnants, pulsar wind nebulae and binary systems, and extragalactic sources such as Gamma-Ray Bursts (GRBs) and Active Galactic Nuclei (AGNs). Among extragalactic sources, GRBs are short-lived bursts of γ-ray photons which last from a few milliseconds to several minutes, while AGNs can constantly emit for a very long period ($> 10^7$ yr), making them one of the most powerful long-lived objects in the Universe. AGNs are a wide range of objects having strong non-thermal emission in the core of their galaxy but having different structure, spectral properties, etc. In the current unified models of AGNs, there is a central supermassive black hole which is surrounded by an accretion disk which emits in the UV and optical bands and in some cases this accretion disk powers a relativistic jet. Jets are observed in radio-loud AGNs and, depending on their orientation, AGNs have different appearances. When the AGN jet makes a larger jet inclination angle, they appear as radio galaxies, while the most extreme sub-class of AGNs- blazars are seen exactly along the jet axis (a few degrees of inclination angle). Due to the small viewing angle and relativistic motion, the emission in blazars is strongly Doppler boosted – a special situation that makes these sources detectable up to large redshifts; these are responsible for the observed extreme properties that characterize blazars, such as superluminal motion and rapid variability across the electromagnetic spectrum.

Blazar jets are strong sources of nonthermal radiation across the electromagnetic

spectrum and their study is a major and important topic in astrophysics. The best way to study the processes taking place in the jets is via their multiwavelength observation. The large number of currently operating telescopes give a specific local view of the ongoing complex emission processes, and by combining the results from the observations in different bands provides us with a comprehensive view of the jet physics. The interpretation of this data within different scenarios can shed light on the physical processes responsible for particle acceleration and cooling in the jets.

The blazars are often considered as the most likely sources of VHE neutrinos and cosmic rays. Protons are unavoidably accelerated with the electrons in the blazar jet, but a direct test of their presence and energy cannot be done when considering only electromagnetic data. Multimessenger observations have long been considered the next major breakthrough required for the study of extragalactic objects. The recent association of IceCube 170922A with TXS 0506+056 provided the first ever possibility to perform a direct multimessenger study of a blazar jet. When combining the data from different messengers (photons, neutrinos and ultrahigh energy protons) each carrying unique information on physical processes, it gives an in-depth view of the blazar jets, which in its turn, enables testing of different jet emission scenarios. This allows to better understand the complex physics of blazar jets, in particular, related with such fundamental problems as formation, launching, collimation and propagation of jets as well as with their internal properties, such as the location of the jet dissipation region, the particle content and density in the jet plasma and its magnetic field, the physical processes responsible for the particle acceleration and emission, etc. The continuous flow of electromagnetic data and observation of new neutrino events from the direction of blazars creates conditions necessary for further exploration of the physics of blazar jets.

The aim of the thesis

The thesis is devoted to the investigation of the fundamental physical processes taking place in blazar jets through analyzing a large amount of multiwavelength data and combining it with neutrino observations. In particular, the aims are:

- to investigate the origin of broadband emission from bright blazars BL Lac and 3C 454.3 by analyzing optical/UV, X-ray and HE γ-ray data accumulated in the past >10 years.
- to study the spectral changes in the γ-ray spectrum of the powerful blazar CTA 102 during the exceptional active period from 2016 to 2017, during which several strong γ-ray flares were observed.
- to perform a detailed temporal and spectral analysis of the data from *Swift* UVOT/XRT, *NuSTAR*, and *Fermi-LAT* observations of high-synchrotron-peaked BL Lac 1ES 1218+304.
- to investigate the multiwavelength emission properties of newly identified

transient γ-ray source 4FGL J1544.3-0649.

- to build new catalogues with X-ray properties of a large number of blazars using the data from *Swift* and *NuSTAR* observations.
- to perform dissection in space, time, and energy of the region around the IceCube-170922A neutrino alert.
- to investigate the origin of broadband emission from the blazars located in the region around the IceCube-170922A neutrino alert.

Scientific novelty

In this thesis novel methods and approaches are used both for data analysis and theoretical interpretation of the results. Various tools are developed to perform complete analyses of optical, UV, X-ray and γ-ray data, which is crucial for analyzing a large amount of observed data allowing to compare and contrast the source properties observed in different periods. A new method for data visualization is introduced (*SED/Light curve animation*) which is the most efficient way to follow the evolution of source emission in time. A new approach to the investigation of the origin of multiwavelength emission from a relativistic blazar jet is introduced. Through combining the analyzed data, 362 high-quality and quasi-simultaneous spectral energy distributions (SEDs) of 3C 454.3 in 2008-2018 are assembled, which have all been modelled within a one-zone leptonic scenario to study the quiescent and flaring states of the powerful blazar 3C 454. Through such an extensive modeling, the underlying emission mechanisms in the 3C 454.3 jet are constrained, allowing to derive the physical parameters of the jet and investigate their evolution in time. By a similar extensive modeling of 511 high-quality and quasi-simultaneous broad-band SEDs of BL Lac, its widely changing multiwavelength emission is systematically investigated. It is shown that the transition of the source's synchrotron component to higher frequencies during the brightest X-ray flare is due to the emergence of synchrotron emission from freshly accelerated particles in a second emission zone located beyond the broad line region.

Through analyzing the multiwavelength data, the existence of a population of still undiscovered blazars (transient blazar) that can occasionally flare and become strong X-ray and γ-ray sources was proposed. In particular, it is shown the remarkable behavior of 4FGL J1544.3-0649 which raised from the state of an anonymous mid-intensity radio source, having never been detected at high energies, into that of one of the brightest extreme blazars in the X-ray and γ-ray sky.

It is shown that the emission from high synchrotron-peaked BL Lac object 1ES 1218+304 is sometimes characterized by an extremely hard (< 1.8) photon index in the X-ray band, indicating that the peak of the synchrotron component was above 1 keV, and so it behaved like an extreme synchrotron BL Lac. A detailed analysis of the *Fermi-LAT* data has shown

that in several periods the γ-ray spectrum of CTA 102 is not consistent with a simple power-law, having a hard photon index that shows a steepening above several GeV. It is shown that this cut-off and break are likely due to a similar intrinsic break in the energy distribution of emitting particles which was used to investigate the origin of the broadband emission from this source.

By systematic processing of all blazar observations of the *NuSTAR* public archive, the first hard X-ray spectroscopic catalogue of blazars (*NuBlazar*) was released. This catalogue is crucial for understanding the physics of blazars. By analyzing all the *Swift*-XRT data and combining the results with multi-frequency data, a complete radio-flux-density-limited sample of HBL was selected.

Using the multiwavelength data for the sources in the region around the IceCube-170922A neutrino alert it is shown that PKS 0502+049 contaminates the γ-ray emission region at low energies, but TXS 0506+056 dominates the sky above a few GeV and the multimessenger diagnostics supports a single coherent picture in which TXS 0506+056 is the only counterpart of all the neutrino emissions in the region. It is shown that neutrino emission from TXS 0506+056 can be produced from inelastic interactions of the jet-accelerated protons in a dense gaseous target. Similar modeling of the PKS 0502+049 multi-wavelength SED showed that, when the neutrinos were observed, its broadband emission was most likely of a leptonic origin.

Practical importance

The results obtained from the studies of individual objects have a wider application for studying the physics of relativistic jets. The introduced new method based on modeling of a large number of quasi contemporaneous SEDs from single source observations is unique and provides an insight into the dynamical changes of the processes at work in blazar jets. The application of this method revealed changes in the jet and emitting electrons causing the multiband frequent flaring activities in the powerful blazar 3C 454.3. These results can be used in particle acceleration simulations to compare and contrast the results from observations with real acceleration mechanisms. Similarly, the fitting of the SEDs of BL Lac observed during 2008-2021 shows that the overall emission from BL Lac from time to time is produced from two regions separated in the jet. The multi-zone emission regions can be formed in different scenarios and their comparison with the parameters obtained here can help to identify the nature of the emitting regions. Understanding of the particle acceleration and cooling processes in synchrotron extreme BL Lac objects represents a major challenge. In this context, identification of some periods, when the X-ray photon index of 1ES 1218+304 became extremely hard (< 1.8), is important for studying the processes in the traditional HBL sources which occasionally turn into extreme synchrotron sources. In blazar jets the location of emission region is an open problem. Identification of

the break in the γ-ray spectrum of CTA 102, a related discussion and the obtained results can be used to infer the distance of emitting region through γ-ray observations. The selected radio-flux-density-limited sample of HBL is important for studying individual blazars as well as the distribution of different types of blazars. The *NuBlazar* catalogue which contains the properties of blazars in hard X-ray bands can be used to study the processes in different blazars. The methods used to identify TXS 0506+056 as the counterpart of the IceCube-170922A neutrino alert can be applied to study the regions around other neutrino events observed by IceCube. The *pp* interaction scenario proposed to explain the neutrinos from the TXS 0506+056 jet has a wider application and can be applied to other blazar jets.

Basic results to be defended:

1) The broadband emission from 3C 454.3 during 2008-2018 is investigated by identifying several active emission states that display the extraordinary flares in the optical/UV, X-ray and γ-ray bands. In the γ-ray band, in several occasions the apparent isotropic γ-ray luminosity exceeded $10^{50} erg\ s^{-1}$. The multiwavelength SEDs of 3C 454.3 (in 362 periods) constrained with contemporaneous data collected during 2008-2018 have been modeled within a one-zone leptonic scenario taking into account the inverse Compton scattering of synchrotron, disk and broad line region (BLR) reflected photons. Through modeling, the main parameters describing the jet in different periods have been estimated, providing an insight into the jet evolution in 2008-2018. It is shown that during the large γ-ray flares, the Doppler boosting factor substantially increased, which points that the emission during the flares comes most likely from a region which either moves faster or has a different geometrical orientation.
2) The long-term (thirteen-year-long) multiwavelength study of the peculiar blazar BL Lac was performed by identifying very different states of the source emission and revealing the complex and high-amplitude variability of the source. Through analyzing the X-ray data, two major X-ray flaring activities were identified showing that during the flare observed on MJD 59128.18 (06 October 2020) the flux increase was associated with the X-ray photon index softening to 2.84 ± 0.03, resulting in the shift of the synchrotron peak to higher frequencies. There are found additional 38 periods when the X-ray photon index softens, extending the X-ray emission beyond the synchrotron component extrapolated from the optical/UV band. Through theoretical modeling it is shown that most of the time the broad-band emission of the source can be described within a simple one-zone scenario when the emission region is inside the BLR, considering the Inverse-Compton up-scattering of both synchrotron and BLR reprocessed photons. In the periods when the X-ray emission is associated with a soft spectral index and when VHE γ-rays were observed, the data could be modeled only considering a second emitting region

outside the BLR. The modeling shows that, depending on the magnetic field and the U_e/U_B ratio, the radiative signature of the second emitting region contributes to either the X-ray or VHE γ-ray bands.

3) By multiwavelength monitoring of 1ES 1218+304 it is shown that in the X-ray band in some *Swift XRT* observations the source emission appeared with an extremely hard photon index of ≤ 1.8 shifting the X-ray spectrum toward higher frequencies, making 1ES 1218+304 an episodic extreme synchrotron blazar. It is shown that broadband emission of the source can be modeled as synchrotron self-Compton emission from the electron population producing the radio-to-X-ray emission in the jet. The power-law exponential cut-off spectrum of emitting electrons required for the SED modeling can be formed when time-limited power-law injection of electrons cool in the emitting region. The value of cut-off energy depends on the time for which the system evolves and $\gamma_{cut} = (4.73 \pm 0.34) \times 10^5$ obtained from the SED modeling can be naturally obtained when the dynamical evolution of the system is $3 - 4\,R/c$ which is in agreement with the absence of flaring activities in the γ-ray band in short time scales.
4) It is shown that during the bright γ-ray flares of CTA 102 observed from 2016 to 2017, the source's γ-ray spectrum is not consistent with a simple power-law, having a hard photon index with an index of $\sim(1.8 - 2.0)$ and showing a spectral cut-off around the observed photon energy of $\sim(9 - 16)$ GeV. Moreover, the estimated cut-off energy remains relatively unchanged when taking the uncertainties into account. It is shown that this cut-off is likely due to a similar intrinsic break in the energy distribution of emitting particles and through modeling of the SED considering a different location for the emitting region the parameters of the emitting electrons are estimated providing important information on the particle acceleration in the jet of CTA 102.
5) By analyzing the data from optical/UV, X-ray and γ-ray observations of 4FGL J1544.3-0649, the existence of a population of still undiscovered objects (transient blazars) that can occasionally flare and become strong X-ray and γ-ray sources was proposed. By analyzing the multiwavelength data it is shown that this source remained undetected at high energies until May 2017 when it showed a transient-like behavior, brightening to such a level as to be detected by the *Fermi*-LAT and the MAXI X-ray sky monitor.
6) By analyzing all the *Swift* X-ray images centered on GRBs and observed during 2004-2019 and combining the survey with multi-frequency data, a complete radio-flux-density-limited sample of high energy peaked blazars (HBL) was selected. By systematically processing all the X-ray data from the *NuSATR* observations of blazars, the first hard X-ray spectroscopic catalogue of blazars (*NuBlazar*) was released. The catalogue, updated to September 30th, 2021, includes 253 observations of 126 distinct blazars, 30 of which have been multiply observed. For each source the corresponding X-ray properties are derived from the data best-fit which are included in the catalogue.

7) By multimessenger investigation of the region around the IceCube-170922A neutrino alert a single coherent picture is found in which the VHE γ-ray blazar TXS 0506+056 is the only counterpart of all the neutrino emissions in the region and therefore the most plausible first non-stellar neutrino and, hence, cosmic ray source. It is shown that the γ-ray emission from TXS 0506+056 during IceCube-170922A event is characterized by a high flux and a soft photon index while a low flux and a hard photon index are found during the neutrino flare in 2014–2015, which shows that TXS 0506+056 has undergone a hadronic flare with very important implications for blazar modeling.
8) A combined leptonic/hadronic scenario for the broadband emission of TXS 0506+056 is proposed. In this scenario, the observed low-energy and time-averaged HE components are explained as an emission directly from the jet- accelerated electrons in a compact region moving with the bulk Lorentz factor of the jet while during the active γ-ray emitting state, when the neutrino was observed, the γ-rays are produced from the inelastic *pp* interactions of the jet-accelerated protons in a dense gaseous target (e.g., clouds from BLR). Through modeling it is shown that if the proton energy distribution is $\sim E^{-2.50}$, and if such a distribution continues up to $E_{c,p} = 10\,PeV$, the expected neutrino rate is as high as ~0.46 events during the long active phase of the source or ~0.15 if the activity lasts 60 days in agreement with the IceCube observations.
9) By analyzing the *Fermi LAT* and *Swift* UVOT/XRT data the origin of multiwavelength emission from PKS 0502+049 neighboring the first cosmic neutrino source TXS 0506+056 is investigated, showing that *1)* the γ-ray spectrum of the source during MJD 56949-57059 is better explained by a power-law model ($\sim E^{-2.07}$) with a cut-off at $E_{cut} = 8.50 \pm 2.06$ GeV which implies the presence of a cut-off in the energy distribution of the parent population of particles responsible for the emission and *2)* the broadband SEDs of the source observed in all periods can be well reproduced by the leptonic models with physically reasonable parameters, unlike the hadronic models, which require a substantially higher jet luminosity. So, the broadband emission from PKS 0502+049 is most likely of a leptonic origin, leaving TXS 0506+056 as the first extragalactic source of VHE neutrinos.

Approbation of the work:

The main results of the thesis had been presented in the following conferences:

1) Recent News from the MeV, GeV and TeV Gamma-Ray Domains, 21-26 March, 2011, Pescara, Italy.
2) THE SUN, THE STARS, THE UNIVERSE and GENERAL RELATIVITY, 11-15 October, 2011, Beijing, China.
3) The Thirteenth Marcel Grossmann Meeting, 1-7 July, 2012, Stockholm, Sweden.
4) The Roma International Conference on Astroparticle Physics, 30 September-03

October, 2014, Noto, Italy.

5) The 6th International Symposium on High-Energy Gamma-Ray Astronomy, 11-15 July, 2016, Heidelberg, Germany.
6) Fifth Bego Rencontre, 15-19 May, 2017, Nice, France.
7) The Third Zeldovich meeting, 23-27 April, Minsk, Belarus.
8) IAU Symposium 342 "Perseus in Sicily: from black hole to cluster outskirts", 13-18 May, 2018, Noto, Italy.
9) MAGIC Extragalactic Working Group meeting, 20-24 January, 2020, Barcelona, Spain.
10) The 17th Italian-Korean Symposium for Relativistic Astrophysics, 02-06 August, 2021, South Korea (online)
11) ICRANet-ISFAHAN Astronomy Meeting, 03-05 November, Iran (online)

Publications

In the topic of the thesis, 41 articles have been published.

Structure of the thesis

The thesis consists of Introduction, nine chapters, Conclusion and References. The thesis contains 261 pages, including 71 figures and 15 tables.

Content of the thesis

In **Introduction,** the literature related to the topic of the thesis is reviewed, the scientific novelty is presented. Also, the main results obtained in each chapter are briefly presented.

In **Chapter 1,** the long-term multiwavelength emission from the powerful blazar 3C 454.3 is investigated by analyzing multiwavelength data. 3C 454.3 is a typical flat spectrum radio quasar (FSRQ) at z=0.859 harboring a black hole with a mass estimated to be $1.5 \times 10^9 M_\odot$. This source was relatively active in all bands, showing several bright flares, and it has become a target of many multiwavelength studies. These multiwavelength campaigns provided unprecedented information on this source.

The γ-ray emission from 3C 454.3 is investigated by analyzing the publicly available *Fermi*-LAT data accumulated between August 4, 2008 and August 4, 2018 in the energy range from 100 MeV to 500 GeV extracted from a 12° region of interest around the γ-ray position of 3C 454.3 (RA=343.497 and Dec=16.149). The flux and photon index variation in time are investigated by computing the light curves in two different ways: the considered period was divided into 3-day bins, but in order to have a deeper and detailed view of the γ-ray flux variation, the light curve was also generated with the help of the adaptive binning method where the bin width is defined by requiring a constant relative flux uncertainty. The light curves computed in both ways are shown in Fig. 1 panels a) and b). The adaptively binned light curve with 20% uncertainty and above $E_0 = 141.6$ MeV is shown in Fig. 1 panel *a)* showing the complex behavior of 3C 454.3 in 2008-2018. The source is so bright that the flux and photon index were estimated in 11698 time intervals,

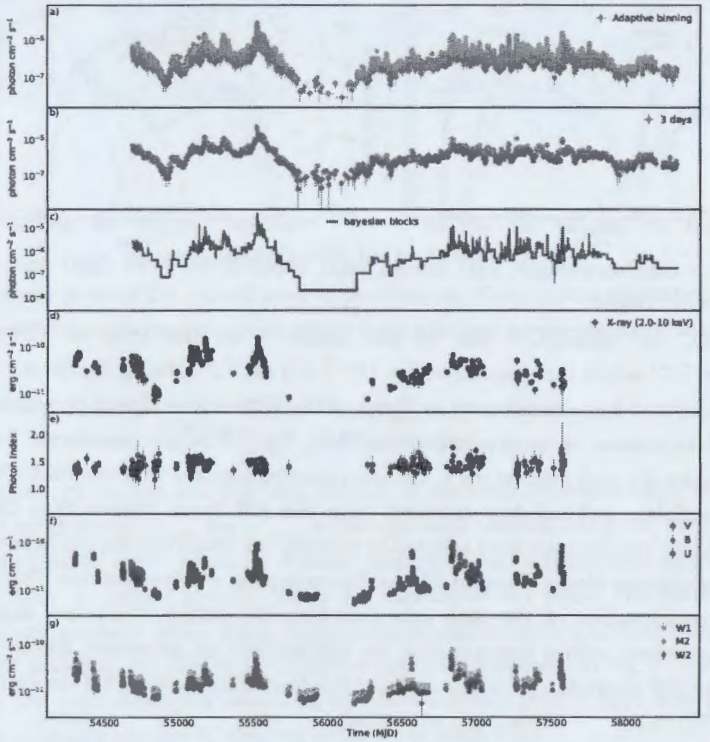

Figure 1: The multiwavelength light curve of 3C 454.3 between 2007 and 2018.

providing a possibility to investigate the γ-ray flux changes also in hour scales. The source exhibited several substantial γ-ray flaring events when the flux increased from $5 \times 10^{-8}\ photon\ cm^{-2}s^{-1}$ (low state) to $> 10^{-5}\ photon\ cm^{-2}s^{-1}$. The major γ-ray flaring activity was observed during MJD 55517-55522 when the highest γ-ray flux of $(9.22 \pm 1.96) \times 10^{-5}\ photon\ cm^{-2}s^{-1}$ was observed on MJD 55519.3 which is 1844 times higher than the lowest γ-ray flux. Interestingly, there are in total 1657 time intervals when the source flux was $> 10^{-5}\ photon\ cm^{-2}s^{-1}$

In the optical/UV and X-ray band, 3C 454.3 was monitored by *Swift* 465 times during 2005 – 2016 and the data collected by XRT and UVOT instruments has been analyzed. Fig. 1 d) shows the 2.0-10.0 keV X-ray flux variation during 2007-2016. The X-ray variation over different observations is evident, the lowest flux being $(7.47 \pm 0.59) \times 10^{-12}\ erg\ cm^{-2}s^{-1}$ and the highest $(1.80 \pm 0.18) \times 10^{-10}\ erg\ cm^{-2}s^{-1}$. Fig. 1 e) shows the variation of the X-ray photon index measured in the 0.3 - 10 keV band. The X-ray photon index is around 1.5 and does not show substantial variation over different observations. Fig. 1 panels f) and g) show the light curves in the optical and UV bands. In

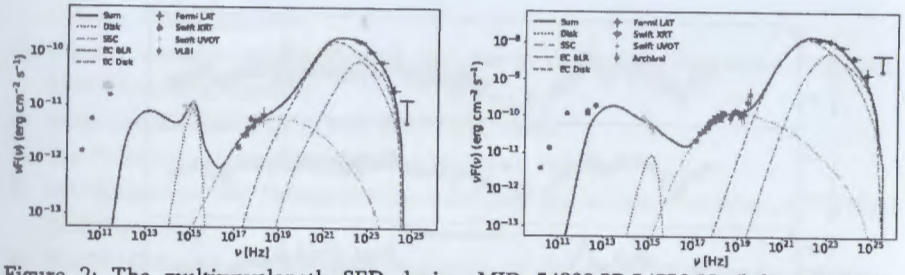

Figure 2: The multiwavelength SED during MJD 54808.37-54750.83 (left) and MJD 55519.59-55520.19 (right).

the low state, the optical/UV flux of the source is at the level of $(7-8)\times 10^{-12}\ erg\ cm^{-2}s^{-1}$ which increases above $3\times 10^{-11}\ erg\ cm^{-2}s^{-1}$ during the flares.

Using the analyzed data, the temporal evolution of the SEDs is investigated by generating SEDs with simultaneous or quasi simultaneous data. The SEDs are constructed in the following manner: for each interval the γ-ray data is plotted together with the *Swift* UVOT, XRT or, if available, archival data extracted from the ASI Space Science Data Centre (ASI/SSDC). The γ-ray intervals were selected by dividing the adaptively binned light curve into piecewise constant blocks (Bayesian blocks) by optimizing a fitness function. This gives the optimal segmentation of the data into time intervals during which the data are statistically consistent with a constant flux. By this method, an adaptively binned light curve produces 388 intervals each with a constant flux level. The resultant SED evolution in time (SED/light curve animation) can be found in https://www.youtube.com/watch?v=wNLVj3W6ZFg showing dramatic changes in the broadband spectrum of 3C 454.3 during 2008-2018.

The obtained multiwavelength data provide unprecedented detailed information on the emission spectrum of 3C 454.3 over different years. When modeling single snapshot SEDs constrained by (quasi) contemporaneous data, the main parameters describing the jet can be estimated, whereas modeling of the SEDs of the same source observed in different periods can provide a clue on the changes in the jet over different periods. Such an interpretation of the data is the backbone of any model aiming to self-consistently explain blazar emission. Thus, all the periods shown in the SED/light curve animation, when the data in the optical/UV, X-ray and γ-ray bands are available (362 periods), have been modeled within a homogeneous one-zone leptonic scenario where the low-energy component is interpreted as synchrotron emission of relativistic electrons, while the second component is due to inverse Compton up-scattering of photons from the jet itself (SSC model), and those from the accretion disk (external Compton scattering of direct disk radiation, EC disk) or those reflected from the BLR clouds (EC BLR). In this interpretation, the emission is produced in a spherical blob of the jet with a size of R filled with uniform magnetic field B that moves

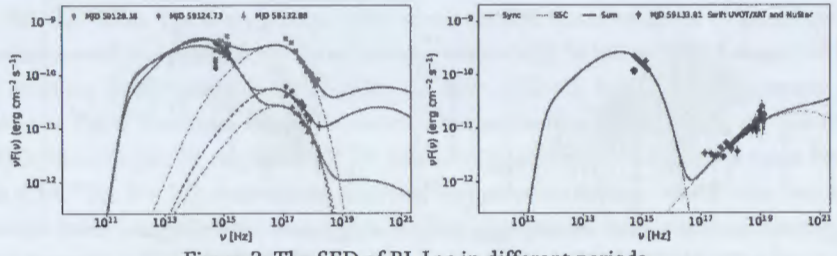

Figure 3: The SED of BL Lac in different periods.

with a Lorentz factor of Γ at a small angle to the observer. The emission region is filled with a population of non-thermal electrons which have a broken power-law distribution in the form of

$$N(\gamma')=\begin{cases} {N_e\gamma'}^{-p_1} & {\gamma'}_{min}\le\gamma'\le{\gamma'}_{br} \\ {N_e\gamma'}_{br}^{\,p_2-p_1}\,\gamma'^{-p_2} & \gamma'>{\gamma'}_{br}\end{cases}$$

where $p1$ and $p2$ are the low and high indexes of electrons correspondingly below and above the break energy ${\gamma'}_{br}$, and ${\gamma'}_{min}$ is the minimum electron energy in the jet frame. The adopted model with physically realistic parameters can satisfactorily reproduce the observed SEDs in various periods during the considered ten years. The results of the modeling are available here: https://www.youtube.com/watch?v=dAqVjpO5Nb4. As an example of modeling, the SED in two different periods is presented in Fig. 2. Through the modeling, the main parameters describing the jet in different periods have been estimated providing an insight into the 3C 454.3 jet evolution in 2008-2018.

In **Chapter 2,** the extensive observations of BL Lac objects prototype BL Lacertae (BL Lac) in the optical, ultraviolet, X-ray and γ-ray bands in a period of nearly 13 years (2008-2021) is used to investigate the origin of its multiwavelength emission. At z=0.069, BL Lac is well known for its prominent variability in a wide energy range, especially in the optical and radio bands. BL Lac has been a target of many multiwavelength campaigns ranging from the radio to the HE or VHE γ-ray bands which resulted in a deep understanding of its properties in different bands.

By analyzing the γ-ray data accumulated between 04 August, 2008 and 01 March, 2021 and generating the light curves, it is shown that the mean γ-ray flux of the source is $4.46\times 10^{-7}\ photon\ cm^{-2}s^{-1}$ which increases up to $(4.39\pm 1.01)\times 10^{-6}\ photon\ cm^{-2}s^{-1}$ (above 196.7 MeV) observed on MJD 59231.34 (17 January 2021). Using the adaptively binned light curve in the considered thirteen years the source flux was above $10^{-6}\ photon\ cm^{-2}s^{-1}$ in total for 41.5 days. The photon index variation in time is investigated using a 3-day binned light curve. The photon index is mostly soft with a mean value of $\Gamma_{mean}=2.15$, but occasionally it hardened to of $\Gamma_{mean}<2.0$. The hardest indexes of 1.48 ± 0.22 and 1.61 ± 0.17 were observed on MJD 57771.16 (18 January 2017) and

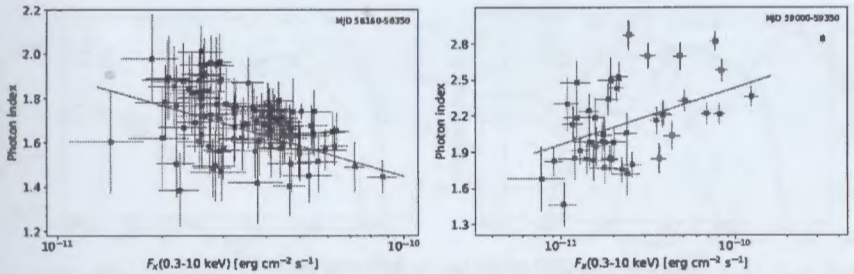

Figure 4: BL Lac X-ray photon index versus the flux during two major X-ray flares. The correlation trend is shown with a red line.

55782.16 (09 August 2011), respectively. In the X-ray band the flux substantially increased in three periods, MJD 56300 (08 January 2013), MLD 59140 (18 October 2020) and MJD 59235 (21 January 2021) reaching the maximum of $(1.41 \pm 0.06) \times 10^{-10}\ erg\ cm^{-2}s^{-1}$ on MJD 59128.18 (06 October 2020). This is the historical highest flux of BL Lac in the soft X-ray band. Most of the time, the photon index is hard (≤ 2.0), implying that the X-ray emission is due to the rising part of the HE component in the SED of BL Lac. However, the photon index undergoes interesting modifications, reaching 2.0, which corresponds to a flat distribution in the $\nu F\nu$ vs ν representation. For example, such tendency is observed after the X-ray flare around MJD 56300 (08 January 2013). In the considered periods, also a significant softening of the photon index is observed; e.g., in 36 observations the X-ray photon index is > 2.3 (considering only the observations when the number of counts was > 100) which is unusual for BL Lac and more typical of high synchrotron peaked blazars. Examples of optical/UV and X-ray spectrum of BL Lac during such changes are shown in Fig 3. The X-ray component started to soften starting from MJD 59113.16 (21 September 2020) when an index of $\Gamma_X = 2.43 \pm 0.11$ was observed. Then, the photon index softens to $\Gamma_X = 2.48 \pm 0.03$ on MJD 59128.18 (06 October 2020) during the brightest X-ray emission state (light blue squares in Fig. 3). In this period the optical/UV flux increased substantially as well, showing that the low-energy component now extends to the X-ray band. Such soft X-ray emission with $\Gamma_X = 2.82 \pm 0.07$ and a flux of $F_x(0.3 - 10\ keV) = (7.68 \pm 0.47) \times 10^{-11}\ erg\ cm^{-2}s^{-1}$ (red circle in Fig. 3) was also observed on MJD 59128.91 (06 October 2020). In the next two observations (MJD 59129.90 (07 October 2020) and 59131.83 [09 October 2020]), the X-ray flux was constantly decreasing and the photon index was $\Gamma_X = 2.52 - 2.70$. The softest photon index of $\Gamma_X = 2.87 \pm 0.11$ was observed on MJD 59132.88 (10 October 2020; magenta triangles in Fig. 3) when the source flux was $F_x(0.3 - 10\ keV) = (2.44 \pm 0.16) \times 10^{-11}\ erg\ cm^{-2}s^{-1}$. However, this component fades in the next observations (e.g., on MJD 59133.81 [11 October 2020]) and in the X-ray band the usual HE component is observed.

The X-ray flux evolution was further investigated by comparing it with the photon index

in different states. The X-ray photon index versus the flux was investigated by selecting the periods around two major X-ray flares, namely, within MJD 56160-56350 (21 August 2012- 27 February 2013) and MJD 59000-59350 (31 May 2020- 16 May 2021). The results are shown in Fig. 4. The linear-Pearson correlation test applied to the data during the first flare (MJD 56160-56350; 21 August 2012- 27 February 2013) yields -0.45, the p-value being 1.6×10^{-6} for $N = 102$ observations, implying a negative correlation between the flux and photon index, i.e., when the source gets brighter, the photon index decreases (hardens). This behavior has already been observed for many flaring blazars. On the other hand, for the second flare the linear-Pearson test results in 0.47 with a p-value of 0.001 for $N = 45$. This implies that during the X-ray flare the photon index softens, so a softer-when-brighter trend is observed. This shows that two major flares observed in the X-ray band for BL Lac are different by their nature and are caused by different processes.

The assembled multiwavelength data are used to investigate the evolution of the broadband spectrum of BL Lac between 2008 August and 2021 March. To this end, a large number of quasi contemporaneous SEDs were generated by plotting the computed γ-ray spectra together with the data available in all other energy bands in each of the Bayesian intervals selected from adaptively binned light curve. The broad band emission SEDs of BL Lac have been combined to form an animation that is available here: https://www.youtube.com/watch?v=KkI1d4gK_UU. In an effort to understand the processes dominating in the jet in different physical conditions, the broadband emission from BL Lac is investigated by modeling all SEDs with sufficient multiwavelength data, typically those with flux measurements in at least the optical/UV, X-ray and γ-ray bands (511 high-quality and quasi-simultaneous SEDs). All these SEDs are modeled within one and two zone scenarios using the open source package JetSet. The results are available here: https://www.youtube.com/watch?v=J3gOi4STZCA. During these soft states (38 among the selected 511 periods) the source's X-ray emission is driven by a new HBL-like component, which significantly differs from the usual X-ray spectrum of BL Lac. The modeling shows that this component may come from a separate emission zone with specific properties, like the size of the emission region, the population of electrons, etc. As an example, some of the SEDs observed during the soft X-ray emission period are shown in Fig. 3. The new soft component clearly goes beyond the synchrotron radiation constrained by the optical/UV data and is interpreted as synchrotron emission from the second region (dashed line) containing much more energetic particles. For example, the electrons should be accelerated up to $\gamma_{cut} = 1.76 \times 10^4$ with $p = 1.15$ to explain the data observed on MJD 59124.73 (02 October 2020; red line). Similar parameters obtained from the modeling of the SED on MJD 59128.18 (06 October 2020) are $\gamma_{cut} = 1.10 \times 10^4$ and $p = 1.49$ (blue line), but the magnetic field is 7.28 G, significantly higher as compared to the previous case (1.65 G). a large magnetic field is required because of the increase in the X-ray flux (~ 6.11 times)

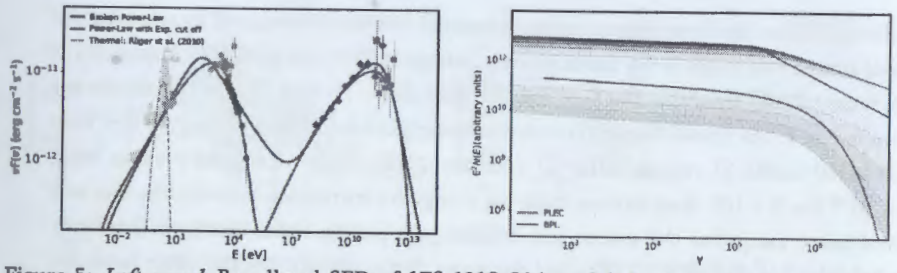

Figure 5: *Left panel:* Broadband SED of 1ES 1218+304 modeled using a one-zone model. *Right panel:* Time evolution of electron spectra considering different initial injection rates.

which cannot be explained by changing γ_{cut}. The X-ray flux variation impacts the magnetic field which decreases to B = 0.27 G on MJD 59132.88 when the soft X-ray component was with a low flux. The electrons in the emitting region are still energetic with $\gamma_{cut} = 5.47 \times 10^4$ but their contribution starts to be subdominant. In fact, the usual hard X-ray component which is interpreted as SSC radiation from the blob inside the broad line region dominates already on MJD 59133.81 (11 October 2020; Fig. 3 right panel).

In **Chapter 3,** the origin of the multiwavelength emission from the high synchrotron peaked BL Lac 1ES 1218+304 is studied using the data from *Swift* UVOT/XRT, *NuSTAR* and *Fermi-LAT*. At z = 0.182, 1ES 1218+304 is an interesting object that was observed in VHE γ-ray band by MAGIC and then by VERITAS telescopes. Its VHE γ-ray emission between 160 GeV and 1.8 TeV is described with a hard γ-ray photon index of 1.72 ± 0.37 after extragalactic background light correction. This emission is most likely produced from fresh accelerated electrons which allows to test various acceleration and cooling processes for the emitting particles, making 1ES 1218+304 an ideal target for exploring the physics of jets.

The γ-ray data from the observation of 1ES 1218+304 from August 2008 to April 2020 were obtained from the data portal and analyzed using the standard analysis procedure provided by the *Fermi-LAT* collaboration. The best match between the model and the data is obtained by the binned likelihood analysis method implemented in *gtlike* tool. In the considered ~11.7 years, 1ES 1218+304 is detected with an overall significance of 77.2σ ($\sigma = \sqrt{TS}$ where $TS = 2(logL_1 - logL_0)$ and L_1 and L_0 are the maximum likelihood values obtained when fitting the observed data using the null and alternative hypotheses, respectively). The best fit results in a relatively hard γ-ray photon index of 1.71 ± 0.02 with a γ-ray flux of $(1.89 \pm 0.09) \times 10^{-8} photon\ cm^{-2} s^{-1}$ in the energy range from 100 MeV to 600 GeV.

Swift observed 1ES 1218+304 116 times between 2008 and 2020. All *XRT* data are analyzed using the *Swift_XRTPROC* pipeline, which is an automatic script for downloading and analyzing *XRT* data. In the X- ray band, the flux gradually increases around MJD 58500 with the highest 0.3-3 keV X-ray flux of $(1.13 \pm 0.02) \times 10^{-10} erg\ cm^{-2} s^{-1}$ on MJD

58499.1, which is by a factor of ~ 5.6 higher than the mean X-ray flux. Similarly, all individual UVOT observations in each filter were analyzed by extracting source counts from a 5″ radius region, while the background was estimated from different positions from a region with a 20″ radius not being contaminated with any signal from the nearby sources. The light curve shows that, like in the X-ray band, also the optical/UV flux shows a few active periods. In the average state the flux in all filters is around $(3 - 5.5) \times 10^{-12} erg\ cm^{-2} s^{-1}$, which strongly increases after MJD 58482 when the absolute highest fluxes of $(2.23 \pm 0.04) \times 10^{-11} erg\ cm^{-2} s^{-1}$ and $(2.05 \pm 0.04) \times 10^{-11} erg\ cm^{-2} s^{-1}$ were observed in M2 and W2 filters on MJD 58486.10 and 58501.20, respectively. The spectra of 1ES 1218+304 in the energy range of 3-79 keV is investigated by analyzing *NuSTAR* data: the photon index is $\Gamma_X = 2.56 \pm 0.028$ and the flux is $(1.21 \pm 0.02) \times 10^{-11} erg\ cm^{-2} s^{-1}$.

The SED of 1ES 1218+304 is modeled in order to gain a further insight of the physical processes at work in its jet. The broadband spectrum of 1ES 1218+304 in the quiescent state is modeled within a simple one zone leptonic scenario, as a large amount of data is available. In this model, the low energy data are interpreted by synchrotron emission of relativistic electrons, while the HE component - as SSC radiation from a compact emitting region. It is assumed that the blob is filled with an electron population in an isotropic magnetic field. For the electron energy distribution, a broken power-law (BPL) and a power-law with an exponential cut-off (PLEC) model were assumed. The SED modeling results are shown in Fig. 5 (left panel) with the corresponding parameters listed in Table 1.

Table 1: Parameters of the models in Fig. 5.

	PLEC (δ = 80)	BPL (δ = 80)
α	2.19 ± 0.04 (2.31 ± 0.03)	2.09 ± 0.06 (2.43 ± 0.02)
α_1	–	3.67 ± 0.10 (4.37 ± 0.15)
$\gamma_{min} \times 10^2$	4.55 ± 0.04 (5.07 ± 0.10)	5.69 ± 0.05 (1.67 ± 0.03)
$\gamma_{cut/break} \times 10^5$	4.73 ± 0.34 (9.57 ± 0.82)	1.72 ± 0.31 (7.47 ± 0.79)
B[G] $\times 10^{-2}$	1.53 ± 0.09 (0.16 ± 0.07)	1.58 ± 0.21 (0.17 ± 0.01)
U_e[erg cm^{-3}]	2.68×10^{-3} (2.24×10^{-3})	2.15×10^{-3} (3.77×10^{-3})
U_B[erg cm^{-3}]	9.31×10^{-6} (9.92×10^{-8})	9.96×10^{-6} (1.13×10^{-7})
L_e[erg s^{-1}]	7.64×10^{43} (6.39×10^{43})	6.11×10^{43} (1.07×10^{44})
L_B[erg s^{-1}]	2.65×10^{41} (2.83×10^{39})	2.84×10^{41} (3.23×10^{39})

The multiwavelength modeling presented in Fig. 5 (left panel) allows to put a constraint on the parameters of emitting electrons. The used BPL and PLEC spectra are an ad-hoc assumption of emitting particles spectrum used for modeling the SED. However, the formation of the particle spectrum is governed by the injection and cooling of electrons. To calculate the temporal evolution of the electron distribution $[N_e(\gamma, t)]$, it is necessary to solve integro-differential equations, describing the losses and injection of relativistic electrons in the emitting region. In this case, the kinetic equation has the following form:

$$\frac{\partial N_e(\gamma,t)}{\partial t} = \frac{\partial}{\partial \gamma}\left(\dot{\gamma} N_e(\gamma,t)\right) - \frac{N_e(\gamma,t)}{t_{esc}} + Q(\gamma,t),$$

where $\dot{\gamma} = d\gamma/dt$ is the radiation loss term, t_{esc} is the characteristic escape time and $Q(\gamma, t)$ is the rate of electron injection. In this case the electrons are predominantly cooled through interaction with magnetic field, so $\dot{\gamma} = -4/3\sigma_T c\, U_B \gamma^2$. In the case of no escape ($t_{esc} \to \infty$), that is all the particles cool inside the emitting region, a BPL spectrum of the electrons will be formed when the power-law index changes as $\alpha_1 - \alpha = 1$. The break energy will be defined by equating the cooling time with the evolution time of the system. In Fig. 5 (right panel) the evolution of the spectrum when the particles are constantly injected ($t_{esc} \gg t_{cool}$) into the emitting region with $Q(\gamma) \sim \gamma^{-2.09}$ is shown for different dynamical time scales; the red gradient shows the spectrum with increasing time. After the system evolves up to $\sim 1.80 \times 10^7$ sec, a break at $\sim 1.72 \times 10^5$ will be formed in the spectrum; for shorter times, the break is at higher energies. However, as expected, the transition at the break energy is smooth ($2.09 \to 3.09$) which cannot explain the estimated electron spectrum obtained from the data modeling (blue spectrum in Fig. 5 [right panel]). Most likely, this break is due to the characteristics of the acceleration processes and for an unknown reason the change in the electrons spectrum is $\Delta\alpha > 1$. Or alternatively, the inhomogeneities in the emitting region could also cause a stronger change in the emitting electron spectrum, which might produce BPL spectrum of electrons with $\Delta\alpha > 1$. Alternative to BPL, a PLEC spectrum can be formed as a result of time averaging of the injected particle spectrum, i.e., after the abrupt power-law injection of the particles ($t_{inj} < t_{cool}$) they start to cool in the emitting region. In time, the HE tail of the particle distribution steepens and a cut-off will be formed. In order to demonstrate this, it is assumed that the $Q(\gamma) \sim \gamma^{-2.19}$ injection of the particles stops at $R/10\,c$ and then the electron distribution evolution up to $10\,R/\,c$ is followed by setting $t_{esc} = 1.5R/\,c$ and $B = 1.53 \times 10^{-2} G$. The blue gradient in Fig. 5 [right panel] corresponds to the electron spectrum calculated for different time intervals. Initially, only the HE electrons ($\gamma > 10^6$) cool or escape the region, declining the injected electron spectrum only at higher energies. Then, with the time the cut-off energy moves to lower energies and after $3 - 4R/\,c$ the break is at the same level as that estimated from the data modeling (1.58×10^5). In principle, by changing the parameters (injection and escape times, etc.), it is possible to satisfactorily reproduce the PLEC spectrum of electrons with the parameters given in Table 1.

In **Chapter 4**, a detailed investigation of the γ-ray emission from CTA 102 during the flaring period is performed. CTA 102 is one of the bright blazars observed by the *Fermi*-LAT in the HE γ-ray band. Even with its large distance, z=1.037, CTA 102 sometimes shows a strong γ-ray outburst with a flux exceeding $10^{-5} photon\ cm^{-2} s^{-1}$. The γ-ray spectrum of CTA 102 is investigated by performing spectral and temporal analyses of the data accumulated from 1 January 2016 to 1 April 2018, when the large-amplitude flaring activities of CTA 102 occurred. The CTA 102 spectra in the 0.1–300 GeV band are analyzed to identify the periods where the spectrum significantly deviates from a simple power-law

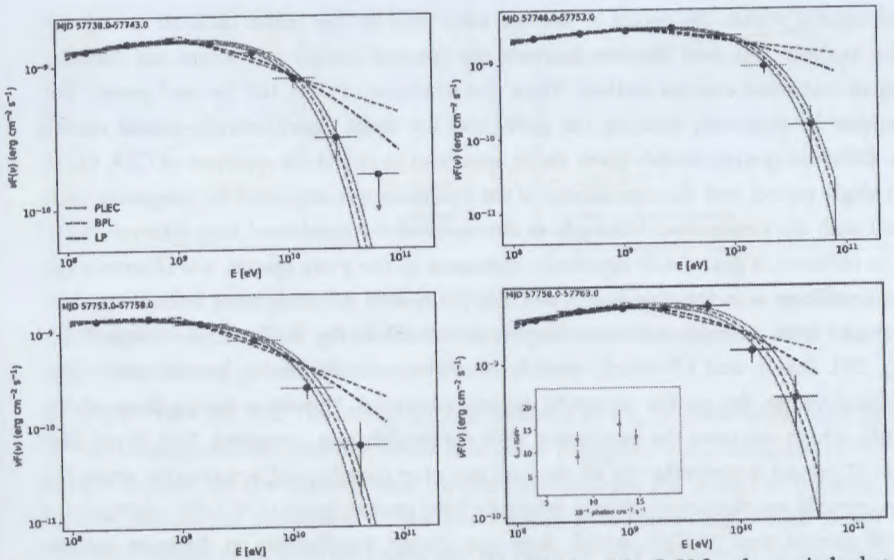

Figure 6: γ-ray spectra in the energy range from 100 MeV to 300 GeV for the periods that showed significant deviation from the simple power-law model.

model. For this reason, the data with different time binning (from one to six days) were analyzed. Only the periods in which a harder photon index was observed were considered further (e.g., $\Gamma \leq 2.1$). This allows selecting only the periods exhibiting substantially different properties, as compared with those observed in the quiescent state, from the flaring states. Among the selected periods, when the power-law model explains reasonably well, the observed data have been excluded, so there remain only the periods in which a hint of a possible deviation from a power-law model is present. Then, in order to check for a statistically significant curvature in the γ-ray spectrum, an alternative fit with the following functions were considered as follows: a power law with an exponential cut-off (PLEC) in the form of

$$dN(E)/dE = N_0 (E/E_0)^{-\Gamma} \exp(-E/E_c)$$

a log-parabola (LP), defined as

$$dN(E)/dE = N_0 (E/E_0)^{-\alpha - \beta \ln(E/E_0)}$$

and a broken power law (BPL), defined as

$$dN(E)/dE = \begin{cases} (E/E_b)^{\Gamma_1}, & if\ E > E_b \\ (E/E_b)^{\Gamma_2}, & if\ E > E_b \end{cases}$$

Different models were compared using a log likelihood ratio test when the significance was estimated as twice the difference in the log-likelihoods. The spectral parameters of CTA 102 were considered as free parameters during the analyses, while the photon indices

of all sources within the region of interest were fixed to the values obtained during the entire analysis. The best matches between the spectral models and events are obtained using an unbinned analysis method. Then, the spectrum of CTA 102 for each period was calculated by separately running the *gtlike* tool for equal logarithmically-spaced energy bins. Different spectral models given above were used to model the spectrum of CTA 102 in each single period, and the significance of the curvature was estimated by comparing each model with the power-law. Although, in almost all of the considered time intervals (from one to six days), a statistically significant curvature in the γ-ray spectra was observed; the most significant is in five-day bins. The CTA 102 spectra deviating from a simple power-law model with a significance exceeding 5σ are shown in Fig. 6. The data fit with PLEC (red), BPL (blue), and LP (black) models are shown. As the fitting provides only log-likelihood values, the models cannot be directly compared. Therefore, the goodness of the fit (χ^2), which compares the data points with the models, was computed. This shows that the PLEC model is preferable for all the periods; other models yield a noticeably worse fit. These periods are characterized by a relatively hard photon index ($\Gamma = 1.84 - 1.98$) and a cut-off around tens of GeV, which does not change significantly in different periods ($E_{cut} = 9.40 - 16.12$ GeV). The variation of E_{cut} with the flux is shown in the inset of the lower panel in Fig. 6. In the considered period, the flux and the cut-off do not vary significantly. A similar conclusion can be drawn when the BPL model is considered (although it fails to explain the data observed at higher energies): The break energy varies around $E_{br} \approx 1.0\ GeV$.

This curvature of the γ-ray spectrum of CTA 102 can be of different origin. In principle, it can be due to absorption when the GeV γ-rays interact with the low-energy photons (through $\gamma\gamma$ collision) or it can be related to similar steepening in the spectrum of the emitting particle distribution due to the interplay of acceleration and cooling processes. Understanding the exact nature of this steepening can help to investigate the processes taking place in the jet of CTA 102 or it can help to localize the γ-ray emitting region. The γ-rays can be absorbed either inside the source, interacting with the photons reprocessed from BLR or during their propagation, interacting with extragalactic background light photons. Considering the distance of CTA 102 (z=1.037), the absorption due to interaction with EBL photons is significant for energies $\geq (200 - 300)$ GeV, as shown in the right panel of Fig. 7 (dot-dashed blue line). Such absorption cannot explain the observed steeping of the spectrum at lower energies. In addition, if the emitting region is inside the BLR, the photons can also be effectively absorbed when interacting with the optical photons. The optical depth was calculated by modeling the BLR as infinitesimally thin spherical shells or thin rings. The luminosity and radius of the shells or rings were estimated using the composite quasar spectrum from the SDSS in terms of L_{H_β}, which is $L_{H_\beta} = (8.93 \pm 6.00) \times$

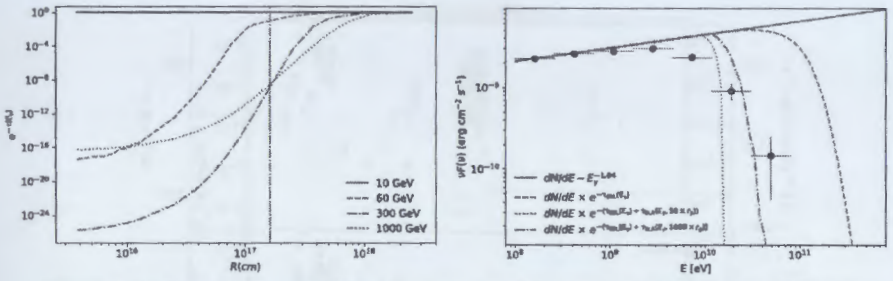

Figure 7*: Left panel:* internal BLR absorption as a function of distance for different γ-ray energies. *Right panel:* reconstructed power-law model compared with the data considering external and internal absorptions.

$10^{43} erg\ s^{-1}$for CTA 102. The absorption is dominated by Ly_α photons at the radii 1.61×10^{17}cm although the absorption by other lines is not negligible. The attenuation ($e^{-\tau(E_\gamma,R)}$) strongly depends on the distance from the central object and the energy of photons. For example, the plot of attenuation versus the distance is shown in Fig. 7 (left panel) for different distances of an emitting region and for photons with energies of 10, 60, 300, and 1000 GeV. The effect of attenuation due to the interaction with BLR photons in the extrapolated power-law spectrum for different distances of the emitting region is shown in Fig. 7 (right panel). These plots show that internal absorption cannot account for the observed curvature. When the emitting region is very deep inside the BLR (e.g., $50 * r_g$), the spectrum steepens quickly, which is in disagreement with the observed data. Whereas for larger distances (e.g. $1000 * r_g$), the slow drop of the flux overproduces the data observed around 10 GeV.

In **Chapter 5**, the results of the analysis of optical/UV, X-ray and γ-ray observations of 4FGL J1544.3-0649, a remarkable blazar showing transient-like HE multiwavelength emission, a behavior that was never observed before in AGNs is presented. This source, in fact, remained below the sensitivity limits of all the HE surveys and observations until May 2017, when it brightened to such a level as to be detectable in short exposures by *Fermi-LAT* and by the MAXI X-ray sky monitor. During the brightening, the 2-10 keV X-ray flux strongly varies, increasing from $(1.0 - 5.0) \times 10^{-12} erg\ cm^{-2} s^{-1}$ to $(1.28 \pm 0.05) \times 10^{-10} erg\ cm^{-2} s^{-1}$. This variability, which is even larger when the flux is estimated in each *Swift* orbit, is clearly associated to a harder-when-brighter behavior. During the γ-ray brightening of the source, the X-ray spectrum modifies as well. The available optical/UV and X-ray data defines the peak of the low-energy component to be within $\nu_{peak-s} = 10^{15} - 10^{17} Hz$, implying 4FGL J1544.3-0649 is a classical HBL. However, occasionally (e.g., on MJD 57898.70, 57989.16, 57998.92, 58009.40 and 58021.40, see here https://www.youtube.com/watch?v=9feaNWi1RDs) the source shows a synchrotron peak

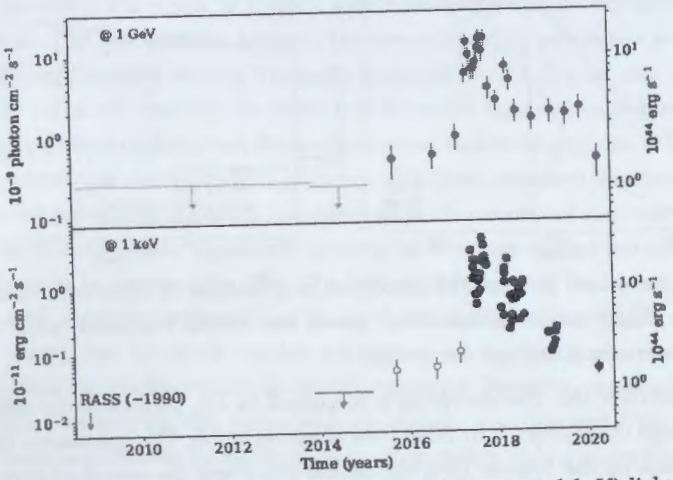

Figure 8: The γ-ray (@ 1 GeV) and the reconstructed X-ray (@ 1 keV) light curve of 4FGL J1544.3-0649 (see text for details).

above $10^{18} Hz$ which is more typical for extreme synchrotron BL Lacs. Yet, in all these periods the γ-ray photon index hardens as well, e.g., 1.74 ± 0.20 on MJD 57898.70, 1.57 ± 0.18 on MJD 57989.16 or 1.61 ± 0.19 on MJD 58021.40, shifting the HE peak to VHEs.

Fig 8 shows the HE light curves of 4FGL J1544.3-0649 spanning the entire operational period of the Fermi mission. The upper panel, reporting the γ-ray data, illustrates the transient nature of this source, which was not detected by the LAT instrument until late 2015, peaked in 2017-2018 and then faded. The lower panel reconstructs the long-term light curve of 4FGL J1544.3-0649 in the X-ray band, combining the *Swift*-XRT measurements (blue points), with the XMM data (red points) and the expected X-ray flux level estimated from the flux in the γ-ray band, based on the average X-ray/γ-ray flux ratio (open grey circles). An upper limit derived from the non-detection of the source in the RASS X-ray sky survey, which was carried out in 1990-1991, is also shown in the leftmost part of the plot. The reconstructed X-ray light curve implies a rise time of approximately two years, and a decay time of approximately three years.

The SED of 4FGL J1544.3-0649 (Fig. 9) assembled with *Swift*-XRT, *Swift*-UVOT, *Fermi-LAT* (green points) and archival data (grey points), shows a highly variable X-ray spectrum, changing its intensity by large factors and often peaking in the X-ray band. For comparison, the average SED of the well-known HBL blazar Mrk501, rescaled to match the radio emission of 4FGL J1544.3- 0649, together with its X-ray spectra observed during its minimum and maximum intensity state, is plotted as light orange points in the same figure.

The nearly identical shape of the radio to optical SEDs and the range of observed X-ray fluxes confirms that 4FGL J1544.3-0649 during the active phase is a typical HBL blazar,

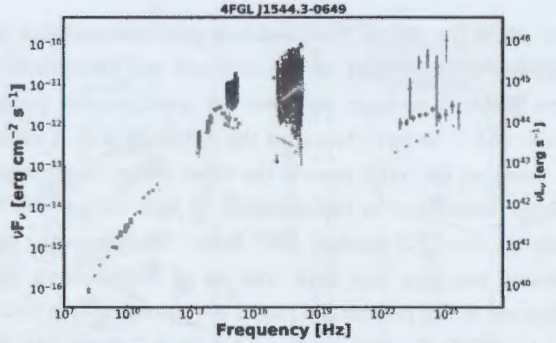

Figure 9: The SED of 4FGL J1544.3-0649.

with X-ray and γ-ray emission that are even stronger than that of Mrk 501. The upper limit from the RASS all sky survey (red arrow) sets the magnitude of the intensity variations in the soft X-ray band, which ranged from below $10^{-13} erg\ cm^{-2} s^{-1}$ in 1990 to such a high value that placed 4FGL J1544.3-0649 amongst the 20 brightest X-ray blazars.

The existence of transient (HBL) blazars was never considered in the literature before the discovery of 4FGL J1544.3-0649 and, consequently, never taken into account in population studies. However, if this dual behavior is relatively common, it might have implications in blazar research, especially in HE and multi-messenger astrophysics, depending on how numerous the transient blazars are and how frequently they enter a bright phase. It is not known if 4FGL J1544.3-0649 represents the tip of the iceberg, or it is simply an isolated event. The identification of similar objects would add crucial information to our knowledge of the population of extragalactic sources, especially in the HE domain. Areas of research that might be affected would be, e.g., the determination of the LogN-LogS, luminosity function and cosmological evolution of HBL blazars, the identification of still unassociated γ-ray and VHE sources, and the contribution of discrete sources to the γ-ray and possibly HE neutrino cosmic backgrounds.

In **Chapter 6,** an X-ray sky survey is performed, using the *Swift* XRT data. All the X-ray images centered on GRB generated by *Swift* over the last 15 years were analyzed using the *Swift_deepsky* Docker container encapsulated pipeline to build the largest existing flux-limited and unbiased sample of serendipitous X-ray sources. Since GRBs explode at random positions in the sky, this survey, after the removal of the target GRBs, constitutes an unbiased medium-deep view of the serendipitous X-ray sky that is suitable for population studies and for the estimation of the cosmological properties of cosmic sources of different types. The main improvement of this survey is a significant increase in the covered area, rather than reaching higher sensitivity. The *Swift*_deepsky software, built on top of the official HEASoft data reduction package, automatically downloads the low-level data and

calibration files from one of the official *Swift* archives, generates exposure maps and X-ray images, detects point-like sources based on the slide-cell and background determination methods built in the XIMAGE package, estimates the count rates in three energy bands (0.3– 1 keV, 1–2 keV, and 2–10 keV) based on the XIMAGE/SOSTA tool; estimates the spectral parameters based on the count rates in the three energy bands considered and on the amount of Galactic absorption in the direction of each source. The *Swift_*deepsky pipeline was run on all the 1332 stacked XRT fields. The processing was completely unsupervised and lasted less than two days. The set of serendipitous point-like X-ray sources that were detected in this process and passed the automatic data cleaning procedure includes 31227 objects, 27740 of which are located at high Galactic latitudes ($|b| > 10^{\circ}$). This sample is a flux-limited unbiased survey of the X-ray sky once the GRB targets of the observations are removed. To identify at least a fraction of our serendipitous X-ray sources, we have cross-matched the OUSXG sample with several astronomical source lists using a matching radius of 10 arcsec for the case of catalogues of point-like objects and 90 arcsec for clusters of galaxies. The catalogue is only available at http://cdsarc.u-strasbg.fr/viz-bin/cat/J/A+A/642/A141.

The X-ray photons provide a wealth of information on the physics of blazars, as in the X-ray band the tail of SED first peak, the rise of the second one or the transition between the two can be observed. *NuSTAR*, thanks to its capability of focusing X-rays up to 79 keV, provides broadband data particularly suitable to compute SEDs in a still poorly explored part of the spectrum. For this reason, systematic processing of all blazar observations of the *NuSTAR* public archive allowed to release the first hard X-ray spectroscopic catalogue of blazars (*NuBlazar*). To compile the list of blazars included in the *NuSTAR* public archive, the Open Universe master list of blazars was cross matched and blazar candidates with the list of all the *NuSTAR* observations carried out before the end of September 2021. *NuSTAR_Spectra* pipeline based on the *NuSTAR* Data Analysis Software (NuSTARDAS), included in the HEASoft V6.29 package, was used to reduce and in a homogeneous and automatic way analyze the selected observations. Using the *NuSTAR_Spectra* pipeline, it is possible to download data, generate high-level calibrated scientific products and perform spectral analyses via a simple command line. As outcomes, *NuSTAR_Spectra* returns the FPMA/B source and background spectra, the corresponding ancillary and response files, the best-fit parameters for a power-law and a logarithmic parabola model, integrated fluxes in the 3-10 and 10-30 keV bands, and the best fit spectral data in $\nu F\nu$ units for SED plotting. Moreover, at the end of the procedure, various plots in .gif format are created to facilitate visual inspection of the results of the analysis and of the generated products. The catalogue resulting from the processing (*NuBlazar*) presents the spectral and observational properties of 126 individual blazars, 30 of which have been multiply observed, for a total of 253 exposures. *NuBlazar* includes 80 LBLs, 32 HBLs and 14 blazars with intermediate SEDs

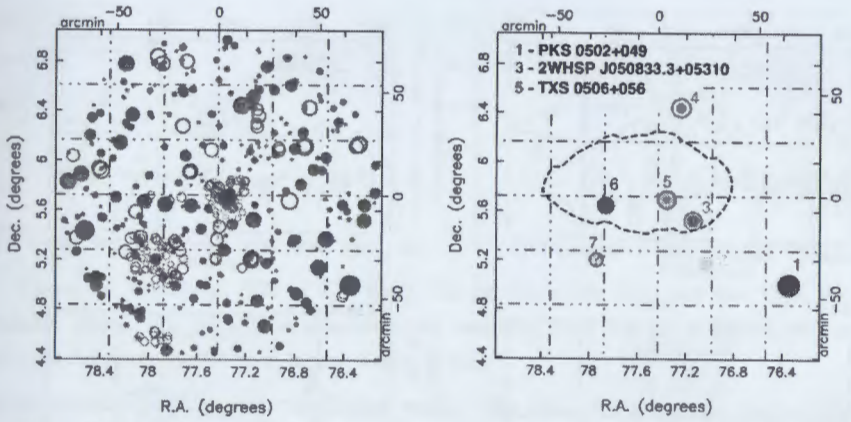

Figure 10: *Left:* Radio and X-ray sources within 80 arcmin of the position of IceCube-170922A. *Right*: Known and candidate blazars around IceCube-170922A.

(IBL). The redshifts of the LBLs cover the range of $0.024 - 4.71$, whereas IBLs and HBLs are relatively nearby with $z < 1$ and $z < 1.2$, respectively. The spectral properties of each object have been derived using a power law and a logarithmic parabola to fit the spectra. The generated catalogue is accessible through web and allows to investigate the properties of the observed sources.

In **Chapter 7,** the dissection in space, time, and energy of the region around the IceCube-170922A neutrino alert is presented. The region around IceCube-170922A neutrino alert is important to explore, since: (1) the first association between a neutrino alert and a blazar in a flaring state– TXS 0506+056; (2) the evidence of a neutrino flaring activity during 2014–2015 from the same direction; (3) the lack of an accompanying simultaneous γ-ray enhancement from the same counterpart; (4) the contrasting flaring activity of a neighboring bright γ-ray source– PKS 0502+049, during 2014 – 2015. The possibility that blazars could be the sources of HE neutrinos has been long discussed in the literature. Following up the IceCube-170922A event observed in coincidence with a γ-ray flare of TXS0506+056, the IceCube collaboration has also detected a neutrino flare in late 2014 – early 2015 from the same direction. Given the complexity of the γ-ray sky in this area, both spatially and temporally, the careful dissection of the region showed the following:

(i) Out of the 637 radio and X-ray sources within 80 arcmin of the IceCube-170922A event position, only 7 are both radio and X-ray emitters and therefore likely non-thermal sources. As it turns out, the X-ray-to-radio flux ratios of these seven sources are blazar-like (see Fig. 10);

(ii) Four of these seven sources are blazars, two of which are very bright γ-ray sources,

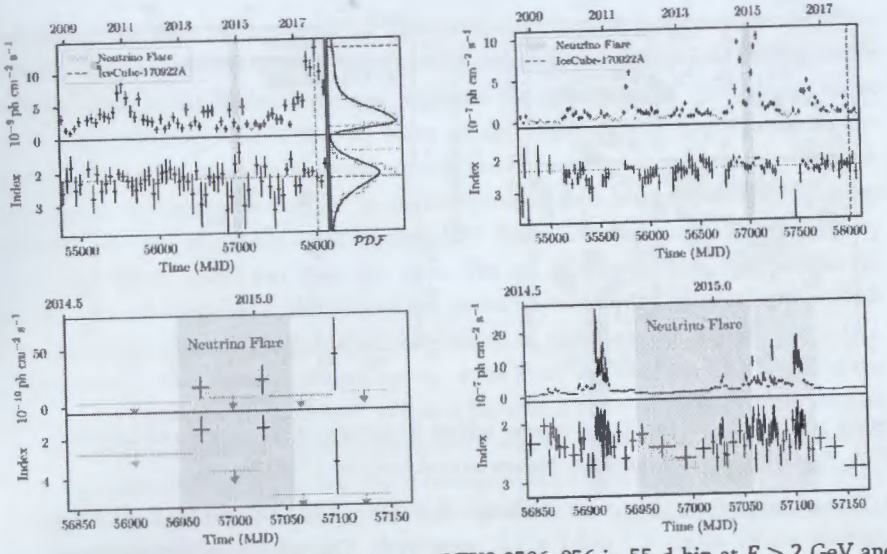

Figure 11: *Left upper:* The light curve of TXS 0506+056 in 55-d bin at $E > 2$ GeV and photon index curve. *Left bottom*: γ -ray flux and photon index of TXS 0506+056 above 10 GeV at the time of the neutrino excess observed around MJD 57000. *Right bottom*: adaptive bin light curve photon flux with Emin = 214 MeV γ -ray light curve of PKS 0502+049 at the time of the neutrino excess observed around MJD 57000.

namely TXS 0506+056 and PKS 0502+049, competing for dominance (see Fig. 10);

(iii) While TXS 0506+056 dominates in all γ-ray bands during the IceCube-170922A event, the situation is more complex during the neutrino flare, as PKS 0502+049 dominates up to $E \sim 1 - 2\ GeV$ but TXS 0506+056 takes over at $E \sim 2 - 5\ GeV$ (see Fig. 11). The γ -ray spectrum of PKS 0502+049, in fact, cuts off at HEs even during flares, a behavior typical of LBL blazars;

(iv) PKS 0502+049 is flaring right before and right after the neutrino flare (but not in coincidence with it) while TXS0506+056 was at its hardest in that time period but in a relatively faint state, suggesting a shift to high energies of the γ-ray SED (see Fig. 11).

The IceCube-170922A event and the neutrino flare at the end of 2014 have been linked to the same source, TXS 0506+056, a blazar of the BL Lac type at z = 0.3365. This is the most plausible association so far between IceCube neutrinos and an extragalactic object. The area near TXS 0506+056 is quite complex due to the presence of several non-thermal sources, which in principle could all contribute to the overall γ-ray flux. By carefully dissecting this region, using a multimessenger approach, it is shown that all spatial, timing, and energetic multimessenger diagnostics point to TXS 0506+056 as the only counterpart of all the neutrinos observed in the vicinity of IceCube-170922A and, therefore, to the first non-

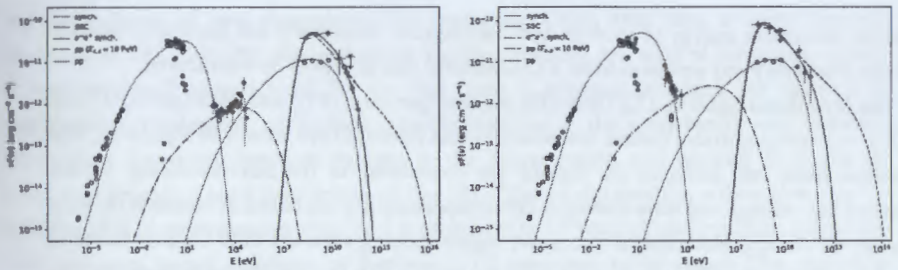

Figure 12: Broadband SED of TXS 0506+056 for the active (left) and low VHE γ-ray emitting states. The boosted synchrotron/SSC emission from the jet is shown in gray, whereas the γ-ray spectra from *pp* are shown in blue.

stellar neutrino (and hence, cosmic-ray) source. The emergent picture is that extreme blazars, i.e. strong, very high energy γ-ray sources with the peak of the synchrotron emission at $> 10^{14} - 10^{15}$ Hz are the first class of sources with an evident contribution to the IceCube diffuse signal.

In **Chapter 8,** the multimessenger processes taking place in the TXS 0506+056 blazar jet are investigated. The HE component in the blazar SEDs can be also explained by applying alternative models invoking the radiative output of hadrons accelerated in the jets of blazars. The protons unavoidably accelerated in the jets can interact with matter *pp*, magnetic, or radiation field (proton–γ) and produce the observed HE emission. In the *pp* interaction scenario, a highly collimated proton beam accelerated in the jet penetrates into a dense and compact target (e.g., cloud(s) from BLR) and produces the observed HE γ-rays through inelastic *pp* scattering. In addition, at larger distances from the nucleus rich in star populations, the star–jet interactions too can produce HE γ-rays. The interaction of the blazar jets with clouds or stars abundant in their environment does not significantly affect the dynamics of the jet and its propagation to kpc scales, but it provides targets for efficient hadronic interactions. The strong shock formed at interaction of relativistic flows with dense targets can accelerate the particles, and in some cases their interactions can be responsible for the steady (e.g., several clouds can interact with the jet simultaneously) or flare-like γ-ray emissions. In the case when the protons interacting in the target produce γ-rays from the decay of neutral pions ($\pi^0 \rightarrow \gamma\gamma$), while the neutrinos ($\upsilon_\mu, \upsilon_e$) are produced from the decay of $\pi^{\pm}$(e.g., $\pi^+ \rightarrow \mu^+ + \upsilon_\mu \rightarrow e^+ + \upsilon_e + \upsilon_\mu + \overline{\upsilon_\mu}$). The observed γ-ray luminosity of TXS 0506+056 around 10 GeV (most likely the peak of HE component) is $4 \times 10^{46} erg\ s^{-1}$, then assuming the efficiency of energy transfer from relativistic protons to secondary particles is ~10%, the required proton luminosity should be $L_p = 4 \times 10^{47} erg\ s^{-1}$. Next, assuming the proton acceleration efficiency is roughly 10%, the jet power would be $L_{jet} = 4 \times 10^{48} erg\ s^{-1}$ - a value usually estimated for bright blazars. Thus,

both the maximum energy of protons and the required luminosity are physically realistic and the observed γ-ray emission from TXS 0506+056 can be due to *pp* interactions.

The broadband SEDs of TXS 0506+056 for low (period 1 [P1]) and high (period 2 [P2]) VHE γ-ray emitting states (when the neutrino was detected) are shown in Figure 12. The emissions from two different jet regions are considered in the SED modeling: (i) the observed low-energy and time-averaged HE components are explained as emission directly from jet-accelerated electrons in a compact region moving with the bulk Lorentz factor of the jet and (ii) during the active γ-ray emitting state, when the neutrino was observed, the γ-rays are produced from the inelastic *pp* interactions in the second emission site. Next, the emission from the e^-e^+pairs produced from the decay of charged pions in the target, which can be significant in the X-ray band, is also taken into account. This modeling allows to estimate both the electron and proton content in the jet. The boosted synchrotron emission from the jet-accelerated electrons can explain the low-energy component, while the SSC radiation of the same electrons - the time-averaged γ-ray data (solid gray line in Figure 12). The γ-rays produced from the decay of π^0 is shown with blue solid and dashed lines in Figure 12. Having calculated the luminosity of protons and their energy distribution, the spectra of HE neutrinos can be calculated straightforwardly and a limit on the expected number of events detectable by IceCube from TXS 0506+056 in a certain exposure time can be obtained. Assuming $t_{exp} = 60\ days$ corresponding to the period when VHE γ-rays from TXS 0506+056 were observed and $t_{exp} = 0.5\ year$ corresponding to the most prolonged active/bright state of the source and assuming $E_{c,p} = 10\ PeV$, the expected neutrino rates during P1 and P2 are correspondingly 0.04 and 0.15 for $t_{exp} = 60\ days$, and correspondingly 0.13 and 0.46 for $t_{exp} = 0.5\ year$. Yet, assuming the proton acceleration continues beyond 10 PeV or the source active phase is longer, the expected rate would be even higher.

Since TXS0506+056 was a poorly studied object before the IceCube-170922A event, an extensive multiwavelength campaign from radio to VHE γ rays on the neutrino blazar candidate TXS 0506+056 was organized. The observations cover the time span from 2017 November (right after the neutrino event of 2017 September) to 2019 February. It is shown that in the VHE γ-ray band, the source showed another days-long flare on the 1-3 of December 2018, observationally very similar (both in the flux level and photon index) to the flare of 2017 September. In the HE γ-ray band, TXS 0506+056 was in a very different state compared to the state in 2017 September: while at that time, the source was in a long-term (on a scale of months) brightening, during this campaign, the source showed a much lower average state with a much faster (days to a week) flaring activity. No significant flares are detected in X-rays or optical/UV. In the radio band, the OVRO observations at 15 GHz revealed the presence of a long-term brightening of the source that increased its flux by

around a factor of two throughout the campaign. Using this data, a lepto-hadronic modeling of TXS 0506+056 was performed, starting from the low state of the source, which is now very well characterized for the first time. A scenario in which the emission is dominated by the leptonic component (inverse Compton in the γ-ray band), with hadronic interactions happening between protons in the blazar region and photons from the jet layer, can provide a good description of the SED. The model predicts a detection rate by IceCube of 0.14 neutrinos per year, or 1.4 neutrinos in 10 years of observations, consistent with the most recent estimates by IceCube (12.3 neutrinos in 10 years). This modeling strengthens the idea that the neutrino emission from AGNs is dominated by their flaring events. The VHE flare of 2018 December does not have simultaneous observations at lower energies, which prevents efficiently constraining the theoretical model. A tentative modeling of these observations, assuming that the only parameters that changed with respect to the low state of the source were the electron and proton primary distributions, is performed. The conclusion is that the γ-ray flare had to be accompanied by a brightening in the optical/UV/X-ray band. Within this model, the associated neutrino emission would have been too rapid and not bright enough to be detected by IceCube (a predicted rate of 2.1×10^{-4} neutrinos per day).

In **Chapter 9,** the origin of the multiwavelength emission from PKS 0502+049 neighboring the first cosmic neutrino source TXS 0506+056 is studied using the data observed by *Fermi-LAT* and *Swift* UVOT/XRT. PKS 0502+049 at z = 0.954 is a bright blazar and is only 1.2° far from TXS 0506+056 and in principle if the neutrinos are produced in the jet of PKS 0502+049 they can have some contribution into the IceCube observed events. The multiwavelength emission from PKS 0502+049 was studied by analyzing the γ-ray data from *Fermi-LAT* and optical/UV/X-ray data from *Swift* UVOT/XRT observations in 2008–2018. In the γ-ray band the source showed several bright periods. The maximum flux of $(4.10 \pm 0.75) \times 10^{-6} photon\ cm^{-2} s^{-1}$ integrated above 100 MeV was observed on MJD 56909.5 within 4.81 h. The evolution of the γ-ray flux during the considered period is shown in Fig. 13 upper panel. During the highest flux, the apparent isotropic γ-ray luminosity is $L_\gamma = 4.72 \times 10^{49}\ erg\ s^{-1}$ (using a distance of $d_L = 6269.5$ Mpc), which corresponds to $L_{em,\gamma} = L_\gamma / 2\delta^2 = 4.72 \times 10^{49}\ erg\ s^{-1}$ (when $\delta = 20$) total power emitted in the γ-ray band in the proper frame of the jet. The γ-ray photon index varies as well, being very soft during the low states while significantly hardening in the bright periods, the hardest one being $\Gamma = 1.82 \pm 0.14$ (Fig. 13 panel b). In the X-ray band, the flux is of the order of a few times $10^{-12} erg\ cm^{-2} s^{-1}$ (see Fig. 13 panel c) but with a hard photon index of $\approx 1.2 - 1.6$, unusual for FSRQs. The X-ray flux variation cannot be tested, as there are only a few observations; however, an evidence of flux increasing around the γ-ray flares can be seen. A similar tendency is present also in the optical/UV data obtained by *Swift* UVOT (see Fig. 13 panel d). The γ-ray spectra when VHE neutrinos were observed as well

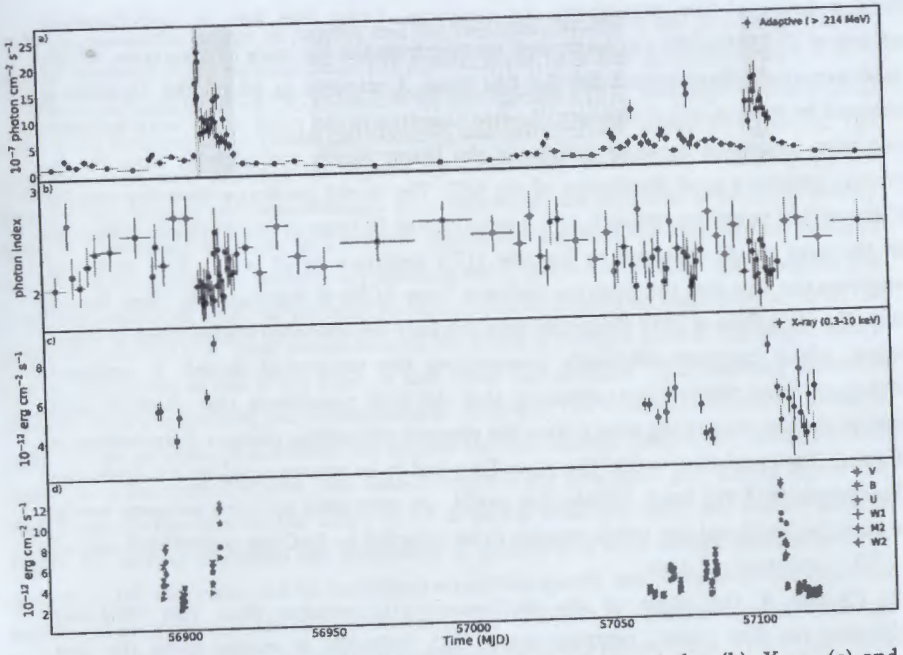

Figure 13: PKS 0502+049 γ-ray light curve (a) and photon index (b), X-ray (c) and optical/UV light curves (d).

as during the γ-ray active periods were obtained. The curved γ-ray emission spectrum during MJD 56949-57059 is better explained by a power-law model ($\sim E^{-2.07}$) with a cut-off at $E_{cut} = 8.50 \pm 2.06\ GeV$. This implies the presence of a cut-off in the energy distribution of the parent population of particles responsible for the emission, so the HE processes were not dominant/efficient in the jet of PKS 0502+049 when the neutrinos were observed by IceCube. When the active periods before and after the neutrinos observation window are considered, the γ-ray emission from PKS 0502+049 appears with a very hard γ-ray photon index of ≤ 2.0. This shows that even if there are certain periods when the jet of PKS 0502+049 was in a favorable state for HE and VHE γ-ray emissions, it seems not to be the case when neutrinos were observed.

The multiwavelength emission from PKS 0502+049 is interpreted within leptonic and hadronic scenarios (Fig. 14). In the hadronic interpretations, the absence of VHE γ-ray data prevents exact estimations of expected neutrino rates when the $p\gamma$ scenario is considered and only quantitative limits can be imposed. In the most optimistic case, the neutrino flux predicted at 100 TeV falls below the IceCube estimated one, implying that the neutrinos accompanying the observed electromagnetic emission (from X- to γ-ray bands) cannot be the source of the observed neutrinos. Next, if the observed γ-rays are due to pp interactions

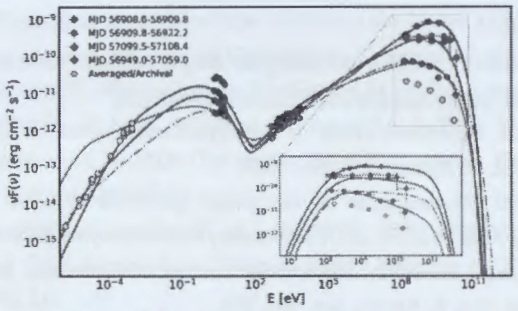

Figure 14: SEDs of PKS 0502+049 during the IceCube observational window (P0; gray) and active states P1 (blue), P2 (red) and P3 (magenta).

in the dense target crossing the jet, then the energy of protons is mostly released in the GeV band allowing a straightforward measurement of the proton spectra based on the observed γ-ray data. The γ-ray data obtained during the IceCube observational window can be well explained when the energy distribution of protons is $E_p^{-2.61}$. Then, if the proton cut-off energy is at ~10 PeV, the maximum possible neutrino detection rate will be ~1.1 events. A higher neutrino detection rate is possible when a harder power-law index of protons $\alpha_p = 2.2$ is considered; however, it strongly overpredicts the HE γ-ray data above 1–2 GeV. Alternatively, a significant neutrino emission is expected during the γ-ray flaring periods when $\alpha_p = 2.1 - 2.2$ and only if $E_{p,c} \geq 100\ TeV$; for example, in order to have a detection rate of > 4.0 events, it is required that the hard γ-ray spectra extend at least up to $E_{c,p}/40 = 2.5\ TeV$; these extreme conditions are hardly possible. In the leptonic interpretations, the broadband spectra of PKS 0502+049 are modeled within the one-zone leptonic scenario assuming the emission is produced in the compact region ($R \leq 5.31 \times 10^{16}(\delta/20)\ cm$ constrained by the observed variability). When the synchrotron/SSC radiation model is considered, the observed data can be explained only when the electron energy density strongly dominates over that of the magnetic field. Instead, the data can be better explained when the inverse Compton scattering of external photons is taken into account; assuming the emitting region is outside the BLR, SSC radiation from the electron population producing the radio-to-optical emission can describe the observed X-ray data, while the emission in the γ-ray band with a large Compton dominance can be explained by the inverse Compton scattering of the dusty torus photons. The presented results and modeling show that the broadband emission from PKS 0502+049 is most likely of a leptonic origin, leaving TXS 0506+056 as the first extragalactic source of VHE neutrinos.

In **Summary,** a brief summary of the obtained results is presented.

PUBLICATIONS IN THE TOPIC OF THESIS

1) Sahakyan N., 2021, *Modelling the broad-band emission of 3C 454.3*, Mon. Not. R.

Astron. Soc. 504, 5074.

2) Sahakyan N., Giommi P., 2022, *A thirteen-year-long broadband view of BL Lac*, Mon. Not. R. Astron. Soc. https://doi.org/10.1093/mnras/stac1011.

3) Sahakyan N., 2020, *Broadband study of high-synchrotron-peaked BL Lac object 1ES 1218+304*, Mon. Not. R. Astron. Soc. 496, 5518.

4) Sahakyan N., 2020, *Investigation of the γ-ray spectrum of CTA 102 during the exceptional flaring state in 2016-2017*, Astronomy & Astrophysics 635, A25.

5) Sahakyan N., Giommi P., 2021, *The strange case of the transient HBL blazar 4FGL J1544.3-0649*, Mon. Not. R. Astron. Soc. 502, 836.

6) Giommi P., Brandt C., Barres de Almeida U., Pollock A., Arneodo F., Chang Y., Civitarese O., De Angelis M., D'Elia V., Del Rio Vera J., Di Pippo S., Middei R., Penacchioni A., Perri M., Ruffini R., Sahakyan N., Turriziani S., 2019, *Open Universe for Blazars: a new generation of astronomical products based on 14 years of Swift-XRT data*, Astronomy & Astrophysics 631, A116.

7) Giommi P., Chang Y., Turriziani S., Glauch T., Leto C., Verrecchia F., Padovani P., Penacchioni A., Arneodo F., Barres de Almeida U., Brandt C., Capalbi M., Civitarese O., D'Elia V., Di Giovanni A., De Angelis M., Del Rio Vera J., Di Pippo S., Middei R., Perri M., Pollock A., Puccetti S., Ricard N., Ruffini R., Sahakyan N., 2020, *Open Universe survey of Swift-XRT GRB fields: Flux-limited sample of HBL blazars*, Astronomy & Astrophysics 642, A141.

8) Middei R., Giommi P., Perri M., Turriziani S., Sahakyan N., Chang Y., Leto C., Verrecchia F., 2022, *The first hard X-ray spectral catalogue of Blazars observed by NuSTAR*, Mon. Not. R. Astron. Soc., stac1185, https://doi.org/10.1093/mnras/stac1185.

9) Padovani P., Giommi P., Resconi E., Glauch T., Arsioli B., Sahakyan N., Huber M., 2018, *Dissecting the region around IceCube-170922A: the blazar TXS 0506+056 as the first cosmic neutrino source*, Mon. Not. R. Astron. Soc. 480, 192.

10) Aartsen M., Ackermann M., Adams J., ... Sahakyan N.... et al. (IceCube Collaboration), 2018, *Neutrino emission from the direction of the blazar TXS 0506+056 prior to the IceCube-170922A alert*, Science, 361, 147.

11) Sahakyan N., 2018, *Lepto-hadronic γ-Ray and Neutrino Emission from the Jet of TXS 0506+056*, The Astrophysical Journal, 866, 109.

12) Acciari V., Ansoldi S., Antonelli L., ...Sahakyan N...., et al. (MAGIC collaboration), 2022, *Investigating the Blazar TXS 0506+056 through Sharp Multiwavelength Eyes During 2017-2019*, The Astrophysical Journal, 927, 197.

13) Sahakyan N., 2019, *Origin of the multiwavelength emission of PKS 0502+049*, Astronomy & Astrophysics 622, A144.

14) Glauch T., Padovani P., Giommi P., Resconi E., Arsioli B., Sahakyan N., Huber M.,

2019, Dissecting the region around IceCube-170922A: the blazar TXS 0506+056 as the first cosmic neutrino source, EPJ Web of Conferences, Volume 207, id.02003.

15) Satalecka K., Bernardini E., Bhattacharyya W., Cerruti M., Fallah Ramazani V., Foffano L., Inoue S., Prandini E., Righi C., Sahakyan N., Tavecchio F. 2019, MAGIC and MWL monitoring of the blazar TXS 0506+056 in the 2018/2019 season, Proceedings of the ICRC 2019 p. 783 (arXiv:1909.04938).

16) Sahakyan N., Yang R., Aharonian F. A., Rieger F. 2013, *Evidence for a Second Component in the High-energy Core Emission from Centaurus A?* The Astrophysical Journal Letters, 770, L6.

17) Sahakyan N., 2012, *High energy γ-radiation from the core of radio galaxy Centaurus A*, Astrophysics, 55, 14.

18) Sahakyan N., 2012, *On the Origin of High Energy Gamma-Rays from Giant Radio Lobes Centarus A*, International Journal of Modern Physics: Conference Series, Volume 12, pp. 224-228.

19) Yang R. Z., Sahakyan N., de Ona Wilhelmi E., Aharonian F., Rieger F., 2012, *Deep observation of the giant radio lobes of Centaurus A with the Fermi Large Area Telescope*, Astro. & Astro. 542, A19.

20) Acciari V., Ansoldi S., Antonelli L., ...Sahakyan N...., et al. (MAGIC collaboration), 2019, *Measurement of the extragalactic background light using MAGIC and Fermi-LAT gamma-ray observations of blazars up to z = 1*, Mon. Not. R. Astron. Soc. 486, 4233.

21) Acciari V., Ansoldi S., Antonelli L., ...Sahakyan N...., et al. (MAGIC collaboration), 2019, Constraints on Gamma-Ray and Neutrino Emission from NGC 1068 with the MAGIC Telescopes, The Astrophysical Journal, 883, 135.

22) Acciari V., Ansoldi S., Antonelli L., ...Sahakyan N...., et al. (MAGIC collaboration), 2019, *Testing emission models on the extreme blazar 2WHSP J073326.7+515354 detected at very high energies with the MAGIC telescopes*, Mon. Not. R. Astron. Soc. 490, 2284.

23) Gasparyan S., Sahakyan N., Baghmanyan V., Zargaryan D., 2018, *On theMultiwavelength Emission from CTA 102*, The Astrophysical Journal, 863, 114.

24) Sahakyan N., Gasparyan S., 2017, *High energy gamma-ray emission from PKS 1441+25*, Mon. Not. R. Astron. Soc. 470, 2861

25) Gasparyan S., Sahakyan N., Chardonnet P., 2018, *The origin of HE and VHE gamma-ray flares from FSRQs*, Int. J. Mod. Phys. D. 27, 1844007

26) Fraga B. M. O., Barres de Almeida U., Gasparyan S., Giommi P., Sahakyan N., 2018, *Time-Evolving SED of MKN421: a multi-band view and polarimetric signatures*, Frontiers in Astronomy and Space Sciences, 5, 1.

27) Barres de Almeida U., Fraga B., Giommi P., Sahakyan N., Gasparyan S., Brandt C.,

2017, *Long-Term Multi-Band and Polarimetric View of Mkn 421: Motivations for an Integrated Open-Data Platform for Blazar Optical Polarimetry*, Galaxies, 5, 90

28) Acciari V., Ansoldi S., Antonelli L., ...Sahakyan N...., et al. (MAGIC collaboration), 2020, *New Hard-TeV Extreme Blazars Detected with the MAGIC Telescopes*, The Astrophysical Journal Supplement Series, 247, 164

29) Acciari V., Ansoldi S., Antonelli L., ...Sahakyan N...., et al. (MAGIC collaboration), 2020, *Unraveling the Complex Behavior of Mrk 421 with Simultaneous X-Ray and VHE Observations during an Extreme Flaring Activity in 2013 April*, The Astrophysical Journal Supplement Series, 248, 29.

30) Acciari V., Ansoldi S., Antonelli L., ...Sahakyan N...., et al. (MAGIC collaboration), 2020, *Monitoring of the radio galaxy M 87 during a low-emission state from 2012 to 2015 with MAGIC*, Mon. Not. R. Astron. Soc. 492, 5354.

31) Acciari V., Ansoldi S., Antonelli L., ...Sahakyan N...., et al. (MAGIC collaboration), 2020, *An intermittent extreme BL Lac: MWL study of 1ES 2344+514 in an enhanced state*, . Not. R. Astron. Soc. 496, 3912.

32) Acciari V., Ansoldi S., Antonelli L., ...Sahakyan N...., et al. (MAGIC collaboration), 2020, *Study of the variable broadband emission of Markarian 501 during the most extreme Swift X-ray activity*, Astronomy & Astrophysics, 637, A86.

33) Acciari V., Ansoldi S., Antonelli L., ...Sahakyan N...., et al. (MAGIC collaboration), *Broadband characterisation of the very intense TeV flares of the blazar 1ES 1959+650 in 2016*, 2020, Astronomy & Astrophysics, 638, A14.

34) Acciari V., Ansoldi S., Antonelli L., ...Sahakyan N...., et al. (MAGIC collaboration), 2020, *Testing two-component models on very high-energy gamma-ray-emitting BL Lac objects*, Astronomy & Astrophysics, 640, A132.

35) Abeysekara A., Benbow W., Bird R..... Sahakyan ...., et al. (MAGIC collaboration), 2020, *The Great Markarian 421 Flare of 2010 February: Multiwavelength Variability and Correlation Studies*, The Astrophysical Journal, 890, 97

36) Acciari V., Ansoldi S., Antonelli L., ...Sahakyan N...., et al. (MAGIC collaboration), 2021, *Multiwavelength variability and correlation studies of Mrk 421 during historically low X-ray and γ-ray activity in 2015-2016*, Mon. Not. R. Astron. Soc. 504, 1427.

37) Acciari V., Ansoldi S., Antonelli L., ...Sahakyan N...., et al. (MAGIC collaboration), 2021, *First detection of VHE gamma-ray emission from TXS 1515-273, study of its X-ray variability and spectral energy distribution*, Mon. Not. R. Astron. Soc. 507, 1528.

38) Acciari V., Ansoldi S., Antonelli L., ...Sahakyan N...., et al. (MAGIC collaboration), 2021, *VHE gamma-ray detection of FSRQ QSO B1420+326 and modeling of its enhanced broadband state in 2020*, Astronomy & Astrophysics, 647, A163.

39) Acciari V., Ansoldi S., Antonelli L., ...Sahakyan N...., et al. (MAGIC collaboration),

2021, *Investigation of the correlation patterns and the Compton dominance variability of Mrk 421 in 2017*, Astronomy & Astrophysics, 655, A89.

40) Algaba J., Anczarski J., Asada K.....Sahakyan N...., et al., 2021, *Broadband Multi-wavelength Properties of M87 during the 2017 Event Horizon Telescope Campaign*, The Astrophysical Journal Letters, 911,446 L11

41) Acciari V., Ansoldi S., Antonelli L., ...Sahakyan N...., et al. (MAGIC collaboration), 2022, *Multiwavelength study of the gravitationally lensed blazar QSO B0218+357 between 2016 and 2020*, Mon. Not. R. Astron. Soc. 510, 2344.

ԱՄՓՈՓԱԳԻՐ

Ատենախոսությունը նվիրված է բլազարների ռելյատիվիստական շիթերում տեղի ունեցող պրոցեսների ուսումնասիրությանը՝ տարբեր ալիքային տիրույթներում գրանցված տվյալների վերլուծության, մաթեմատիկական մոդելավորման և ստացված արդյունքների տեսական մեկնաբանման միջոցով: Հետազոտվել է նաև բլազարների շիթերում տեղի ունեցող հադրոնային պրոցեսները, գնահատվել են նեյտրինոների ճառագայթման հոսքերը և հնարավոր գրանցումը IceCube դիտակով: Ատենախոսությունը կազմված է ներածությունից, ինը գլուխներից, վերջաբանից և հղումների ցանկից:

Ատենախոսությունը սկսվում է ներածությունով, որտեղ ներկայացված են թեմայի արդիականությունը և քննարկվող հիմնական խնդիրները:

Առաջին գլխում ուսումնասիրվել են FSRQ դասի 3C 454.3 բլազարի շիթում տեղի ունեցող պրոցեսները՝ վերլուծելով 2008–2018թթ. ընթացքում գրանցված տվյալները: Ցույց է տրվել, որ օպտիկական, ուլտրամանուշակագույն (ՈւՄ), ռենտգենյան և բարձր էներգիաների (ԲԷ, ≥ 100 ՄէՎ) γ տիրույթներում գրանցվել են մի քանի հզոր բռնկումներ, օրինակ՝ ԲԷ γ տիրույթում ճառագայթման լուսատվությունը աճել է մինչև 2.15×10^{50} էրգ վրկ$^{-1}$: Ցույց է տրվել, որ ռենտգենյան տիրույթում ճառագայթման սպեկտրի ինդեքսը $\Gamma_X = 1.16 - 1.75$ տիրույթում է, իսկ բռնկման վիճակում հոսքը աճել է մինչև $(1.80 \pm 0.18) \times 10^{-10}$ էրգ սմ$^{-2}$վրկ$^{-2}$: Վերլուծված տվյալներով պատրաստվել են աղբյուրի միաժամանակյա տվյալներով ստացված էներգիայի սպեկտրալ բաշխվածությունները (ԷՍԲ), որոնք մոդելավորվել են մեկ տիրույթից լեպտոնային ճառագայթման մոդելի շրջանակում:

Երկրորդ գլխում, վերլուծելով 13 տարիների (2008–2021թթ.) ընթացքում գրանցված փորձարարական տվյալները, հետազոտվել են IBL դասի BL Lac բլազարի շիթում տեղի ունեցող պրոցեսները: Ցույց է տրվել, որ աղբյուրի ճառագայթումը արագ փոփոխվում է օպտիկական, ՈւՄ, ռենտգենյան և ԲԷ γ տիրույթներում: Ռենտգենյան տիրույթում 2020թ. հոկտեմբերի 6-ին գրանցված բռնկման ժամանակ հոսքի աճին զուգահեռ ֆոտոնային ցուցիչը դառնում է (2.84 ± 0.03), ինչի հետևանքով սինքրոտրոնային ճառագայթման բաղադրիչը տեղափոխվում է դեպի ավելի մեծ

հաճախությունների տիրույթ ($\sim 10^{17}$ Հց):

Երրորդ գլխում ուսումնասիրվել են HBL դասի 1ES 1218+304 աղբյուրի ճառագայթման մեխանիզմները՝ իրականացնելով 2008-2020թթ. գրանցված տվյալների ժամանակային և սպեկտրալ վերլուծություն: Ցույց է տրվել, որ որոշ դեպքերում աղբյուրի ռենտգենյան տիրույթում ճառագայթման ֆոտոնային ցուցիչը ≤ 1.81, ինչի հետևանքով աղբյուրի սինքրոտրոնային ճառագայթման բաղադրիչի առավելագույնը շեղվում է դեպի ավելի բարձր հաճախականություններ ($> 10^{18}$ Հց) և աղբյուրը ժամանակավորապես վերածվում է extreme synchrotron բլազարի:

Չորրորդ գլխում, CTA 102-ի ԲԷ γ տիրույթում ճառագայթման սպեկտրի մանրամասն ուսումնասիրությամբ ցույց է տրվել, որ մի քանի ժամանակահատվածներում ճառագայթման սպեկտրը $(9-16)$ ԳԷՎ էներգետիկ տիրույթում շեղվում է պարզ աստիճանային օրենքից: Այդ շեղումը հնարավոր չէ բացատրել լայն գծերով տիրույթից անրադարձած ֆոտոնների հետ փոխազդեցությամբ պայմանավորված կլանումով, և այն, ամենայն հավանականությամբ, պայմանավորված է ճառագայթող մասնիկների սպեկտրում նմանատիպ շեղման առկայությամբ, ինչը հետազոտվել է, մոդելավորելով աղբյուրի ԷՍԲ-ը՝ քննարկելով ճառագայթման տիրույթի տարբեր դիրքեր:

Հինգերորդ գլխում, վերլուծելով 4FGL J1544.3-0649 աղբյուրի օպտիկական, ՈւՄ, ռենտգենյան և ԲԷ γ տիրույթներում գրանցված տվյալները, առաջարկվել է ժամանակավոր (transient) բլազարների նոր դաս: 4FGL J1544.3-0649 աղբյուրը ռադիո տիրույթում ուսումնասիրություններից հայտնի բլազար է, որը չէր ճառագայթում ռենտգենյան և ԲԷ γ տիրույթներում: Ցույց է տրվել, որ 2016-2017թթ.-ից հետո աղբյուրի ճառագայթումը ռենտգենյան և γ տիրույթներում կտրուկ աճել է, և աղբյուրի ճառագայթումը գրանցվել է *Swift* XRT, *MAXI* և *Fermi-LAT* դիտակներով:

Վեցերորդ գլխում, վերլուծելով *Swift* դիտակով վերջին 15 տարիների (2004-2019) ընթացքում գրանցված տվյալները և ստացված արդյունքները համեմատելով բազմահաճախային տիրույթում գրանցված այլ կատալոգների հետ, առանձնացվել են ռենտգենյան տիրույթում ճառագայթող բլազարները, որոնց սինքրոտրոնային ճառագայթման բաղադրիչի առավելագույն հաճախությունն ընկած է $> 10^{15}$ Հց տիրույթում: Վերլուծելով *NuSTAR* դիտակով գրանցված բոլոր բլազարների տվյալները (126 աղբյուր), պատրաստվել է 3-79 կէՎ տիրույթում բլազարների առաջին կատալոգը՝ NuBlazar-ը:

Յոթերորդ գլխում, օգտագործելով բազմահաճախային տիրույթում գրանցված տվյալները, հետազոտվել են IceCube-170922A նեյտրինո ազդանշանի ուղղությամբ գտնվող շրջակա տիրույթում առկա բոլոր աղբյուրների հատկությունները, ցույց է տրվել որ TXS 0506+056 աղբյուրը, որը ռադիոյից մինչև ԲԷ γ տիրույթը շատ հզոր ճառագայթման աղբյուր է, ամենայն հավանականությամբ նաև նեյտրինոների ճառագայթման աղբյուր է, հետևաբար այն նեյտրինոների ճառագայթման առաջին

տիեզերական աղբյուրն է:

Ութերորդ գլխում ուսումնասիրվել է TXS 0506+056 բլազարի շիթում տեղի ունեցող հադրոնային պրոցեսները IceCube-170922A նեյտրինո ազդանշանի գրանցման ժամանակ: Ցույց է տրվել, որ գերբարձր էներգիաների նեյտրինոների ճառագայթման ժամանակ, աղբյուրի γ ճառագայթումը կարող է առաջանալ շիթում արագացված պրոտոնների փոխազդեցությունից, օրինակ՝ երբ շիթը փոխազդում է խիտ թիրախի հետ: Այս դեպքում գրանցված տվյալները կարելի է բացատրել, եթե շիթում արագացված պրոտոնների էներգետիկ բաշխումը նկարագրվում է $E^{-2.50}$ օրենքով, մինչև $E_c = 10$ ՊԷՎ, ապա առաջացած նեյտրինոների հոսքը կարող է բացատրել IceCube դիտակով գրանցված ազդանշանը:

Իններորդ գլխում ուսումնասիրվել են նեյտրինոների ճառագայթման առաջին տիեզերական աղբյուրի երկնային տիրույթին մոտ գտնվող PKS 0502+049 բլազարի բազմահաճախային տիրույթում ճառագայթման մեխանիզմները: Ցույց է տրվել, որ 1) նեյտրինոների ճառագայթման ժամանակ աղբյուրի γ տիրույթում ճառագայթումը շեղվում է պարզ աստիճանային օրենքից $E_c = (8.50 \pm 2.06)$ ԳԷՎ-ից բարձր տիրույթում և 2) նեյտրինոների ճառագայթման ժամանակ PKS 0502+049 աղբյուրից γ ճառագայթումը պայմանավորված էր արագացված էլեկտրոններով:

Резюме

Диссертация посвящена изучению процессов в релятивистских струях блазаров путем анализа и интерпретации многоволновых данных. Также исследуются адронные процессы в струях, оценивая ожидаемый поток нейтрино очень высоких энергий. Диссертация состоит из введения, девяти глав, заключения и списка литературы.

В главе 1 исследовано многоволновое излучение 3C 454.3 в течение 2008-2018 гг. Были идентифицированы вспышки высокой интенсивности в оптическом/УФ, рентгеновском и γ-диапазонах. Например, в γ-диапазоне несколько раз светимость превышала 10^{50}эрг c^{-1}. Многоволновой спектр 3C 454.3 в 362 периодах были смоделированы в рамках однозонного лептонного сценария, предполагающего, что область излучения находится в области широкой линии.

В главе 2 проведено многоволновое исследование пекулярного блазара BL Lac, в ходе которого были выявлены различные состояния излучения источника и выявлена его сложная и высокоамплитудная переменность. Показано, что в рентгеновском диапазоне во время вспышки, наблюдавшейся 6 октября 2020 г., с увеличением потока фотонный индекс был 2.84 ± 0.03, что привело к смещению синхротронного пика на более высокие частоты. С помощью теоретического моделирования показано, что этот компонент производится из второй области излучения.

В главе 3 показано, что источник 1ES 1218+304 в нескольких наблюдениях в

рентгеновском диапазоне имеет фотонный индекс ≤ 1.8 и синхротронный пик был смещен в сторону более высоких частот, что делает 1ES 1218+304 эпизодическим экстремальным синхротронным блазаром. Показано, что многоволновое излучение источника можно смоделировать как синхротронное самокомптоновское излучение от электронов, ускоренных в струе.

В главе 4 проведено детальное исследование γ-спектра CTA 102 с использованием данных *Fermi* LAT. Показано, что в течение нескольких периодов γ-спектр источника имея жесткий фотонный индекс в диапазоне $\sim(1.8-2.0)$ отклоняется от простого степенного закона в $\sim(9-16)$ ГэВ. Показано, что этот отклонение, вероятно, связано с аналогичным внутренним отклонение в распределении энергии излучающих частиц.

В главе 5 было предложено существование популяции транзиентных блазаров, то есть еще не открытых объектов, которые могут время от времени быть активными и становиться сильными источниками. Анализируя многоволновые данные, показано, что 4FGL J1544.3-0649, который не был обнаружен в области высоких энергий до мая 2017 г., в течение нескольких месяцев демонстрировал переходное поведение когда его излучение увеличилось и было обнаружено телескопами *Fermi*-LAT и MAXI.

В главе 6 были проанализированы все рентгеновские снимки *Swift* наблюдавшиеся в течение 2004-2019гг. и сравнивая результаты с многочастотными данными были выбраны высокоэнергетические пиковые блазары. Путем систематической обработки всех рентгеновских данных наблюдений блазаров телескопом *NuSTAR* был подготовлен первый спектроскопический каталог блазаров (NuBlazar) в диапазоне 3-79 кэВ.

В главе 7 изучена область вокруг нейтринного события IceCube-170922A. Показано, что в низкоэнергетическом γ-диапазоне доминирует излучение от PKS 0502+049, но в диапазоне выше нескольких ГэВ доминирует TXS 0506+056. Показано, что TXS0506+056 является единственным источником нейтрино, зарегистрированных в 2017 и 2014-2015гг. и, следовательно, является первым космическим источником нейтрино сверхвысоких энергий.

В главе 8 исследованы лепто-адронные процессы в струе TXS 0506+056. Показано, что наблюдаемое излучение от TXS 0506+056 может быть объяснено синхротронным и обратным комптоновским излучением от струи, но во время излучения нейтрино наблюдаемые данные γ-излучения можно объяснить как неупругое взаимодействие ускоренных струй протонов в плотной газовой мишени.

В Главе 9 было исследовано происхождение многоволнового излучения от PKS 0502+049. Показано, что многоволновой спектр источника, наблюдаемый во все периоды, может быть смоделирован лептонными моделями с физически разумными параметрами, в отличие от адронных моделей, требующих существенно большей светимости струи.